Low levels of nitryl chloride at ground level: Nocturnal nitrogen oxides in the Lower Fraser Valley of British Columbia

Hans D. Osthoff[1], Charles A. Odame-Ankrah[1], Youssef M. Taha[1], Travis W. Tokarek[1], Corinne L. Schiller[2], Donna Haga[3], Keith Jones[2], and Roxanne Vingarzan[2]

[1] {Department of Chemistry, University of Calgary, Calgary, Alberta T2N 1N4, Canada}

[2] {Applied Science Division, Prediction and Services West, Meteorological Service of Canada, Environment and Climate Change Canada, Vancouver, British Columbia V6C 3S5, Canada}

[3] {British Columbia Ministry of Environment and Climate Change Strategy, Cranbrook, British Columbia V1C 7G5, Canada}

Correspondence to: H. D. Osthoff (hosthoff@ucalgary.ca)

Abstract

The nocturnal nitrogen oxides, which include the nitrate radical (NO_3), dinitrogen pentoxide (N_2O_5), and its uptake product on chloride containing aerosol, nitryl chloride ($ClNO_2$), can have profound impacts on the lifetime of NO_x (= NO + NO_2), radical budgets, and next-day photochemical ozone (O_3) production, yet their abundances and chemistry are only sparsely constrained by ambient air measurements.

Here, we present a measurement data set collected at a routine monitoring site near the Abbotsford International Airport (YXX) located approximately 30 km from the Pacific Ocean in the Lower Fraser Valley (LFV) on the West coast of British Columbia. Measurements were made from July 20 to August 4, 2012, and included mixing ratios of $ClNO_2$, N_2O_5, NO, NO_2, total odd nitrogen (NO_y), O_3, photolysis frequencies, and size distribution and composition of non-refractory submicron aerosol (PM_1).

At night, O_3 was rapidly and often completely removed by dry deposition and by titration with NO of anthropogenic origin and unsaturated biogenic hydrocarbons in a shallow nocturnal inversion surface layer. The low nocturnal O_3 mixing ratios and presence of strong chemical sinks for NO_3 limited the extent of nocturnal nitrogen oxide chemistry at ground level. Consequently, mixing ratios of N_2O_5 and $ClNO_2$ were low (<30 and <100 parts-per-trillion by volume (pptv) and median nocturnal peak values of 7.8 pptv and 7.9 pptv, respectively). Mixing ratios of $ClNO_2$ frequently peaked 1 - 2 hours after sunrise rationalized by more efficient formation of $ClNO_2$ in the nocturnal residual layer aloft than at the surface and the breakup of the nocturnal boundary layer structure in the morning. When quantifiable, production of $ClNO_2$ from N_2O_5 was efficient and likely occurred predominantly on unquantified supermicron sized or refractory sea salt derived aerosol. After sunrise, production of Cl radicals from photolysis of $ClNO_2$ was negligible compared to production of OH from the reaction of $O(^1D) + H_2O$ except for a short period after sunrise.

Keywords

Lower Fraser Valley, $ClNO_2$, surface measurements, nocturnal residual layer, $ClNO_2$ morning peak, vertical entrainment

1 Introduction

The Lower Fraser Valley (LFV) is prone to episodes of poor air quality, in part because of its geography which facilitates stagnation periods and accumulation of airborne pollutants through processes such as the Wake-Induced Stagnation Effect (Brook et al., 2004), and also because of continued growth of human population and associated emissions from urban, suburban, agricultural and marine sources. Of special concern have been repeated exceedances of the Canada-Wide Standard and, as of 2012, the Canadian Ambient Air Quality Standards (CAAQS) for fine particulate matter ($PM_{2.5}$) and ozone (O_3) at Chilliwack and Hope, located in the eastern part of the LFV downwind of Vancouver (Ainslie et al., 2013). These exceedances have occurred in spite of ongoing declines in emissions of both nitrogen oxides (NO_x = NO + NO_2) and volatile organic compounds (VOCs) resulting from the introduction of new vehicle standards and (now discontinued) local vehicle emission testing programs (Ainslie et al., 2013). Previous large-scale studies in the LFV such as Pacific 1993 (Steyn et al., 1997), the Regional Visibility Experimental Assessment in the Lower Fraser Valley (REVEAL) I and II (Pryor et al., 1997; Pryor and Barthelmie, 2000) and Pacific 2001 (Vingarzan and Li, 2006) have added important information regarding atmospheric processes leading to O_3 and aerosol formation and visibility issues. However, the transformation of primary (e.g., NO_x, VOCs, SO_2, NH_3, etc.) to secondary pollutants (i.e.., O_3 and fine particulate matter) is highly complex, and the scientific understanding of these highly non-linear processes remains incomplete.

A complicating factor in the LFV is the interaction of anthropogenic emissions with marine derived sea salt aerosol. While sea spray aerosol is a primary source of particulate matter (PM) and hence directly affect particle concentrations and mass loadings (Pryor et al., 2008) and aerosol chloride concentrations (Anlauf et al., 2006) in the LFV, there is now considerable evidence from modeling (Knipping and Dabdub, 2003), laboratory (Raff et al., 2009), and field studies (Tanaka et al., 2003; Osthoff et al., 2008) that "active chlorine" species released from sea salt can negatively affect air quality and promote O_3 and secondary aerosol formation in coastal regions.

In an analysis of 20 years of O_3 air quality data in the LFV region, Ainslie and Steyn (2007) concluded that precursor buildup, prior to an exceedance day, plays an important role in the spatial O_3 pattern on exceedance days. Secondary processes involving active chlorine

produced from the interaction of marine aerosol with anthropogenic pollution would fit this profile but are not currently constrained by measurements.

One pathway to activate chlorine from sea salt is the reactive uptake of dinitrogen pentoxide (N_2O_5) on chloride containing aerosol to yield nitryl chloride ($ClNO_2$) (Behnke et al., 1997; Finlayson-Pitts et al., 1989). Briefly, N_2O_5 is formed from the reversible reaction of nitrogen dioxide (NO_2) with the photo-labile nitrate radical (NO_3; R1), which in turn is formed from reaction of NO_2 with O_3 (R2).

$$NO_2 + O_3 \rightarrow NO_3 + O_2 \quad \text{(R1)}$$

$$NO_3 + NO_2 \rightleftharpoons N_2O_5 \quad \text{(R2)}$$

In ambient air, N_2O_5, NO_3 and NO_2 are usually in equilibrium; the equilibrium constant, K_2, is temperature dependent, favoring NO_3 and NO_2 at higher temperatures (Osthoff et al., 2007). During daytime, NO_3 (and, indirectly, N_2O_5) is removed primarily via its reaction (R3) with NO (which is generated from NO_2 photolysis and directly emitted, for example, by automobiles) and by NO_3 photolysis (R4) (Wayne et al., 1991).

$$NO_3 + NO \rightarrow 2NO_2 \quad \text{(R3)}$$

$$NO_3 + h\nu \rightarrow 0.9NO_2 + 0.1NO \quad \text{(R4)}$$

The heterogeneous hydrolysis of N_2O_5 to nitric acid (HNO_3) is an important nocturnal NO_x and odd oxygen ($O_x = NO_2 + O_3$) removal pathway (Chang et al., 2011; Brown et al., 2006a). On chloride containing aerosol, however, uptake of N_2O_5 yields up to a stoichiometric amount of $ClNO_2$ (R5) (Behnke et al., 1997; Finlayson-Pitts et al., 1989):

$$N_2O_5 + H_2O(het) + \phi Cl^-(het) \rightarrow (2-\phi)HNO_3(het) + \phi ClNO_2,\ 0 \leq \phi \leq 1 \quad \text{(R5)}$$

The $ClNO_2$ yield, ϕ, is primarily a function of aerosol chloride and water content (Behnke et al., 1997; Bertram and Thornton, 2009; Roberts et al., 2009; Ryder et al., 2014; Ryder et al., 2015b; Ryder et al., 2015a). Formation of $ClNO_2$ impacts air quality in the following ways: Since $ClNO_2$ is long-lived at night, its primary fate is photo-dissociation (to Cl and NO_2) in the morning hours after sunrise (R6) (Osthoff et al., 2008).

$$ClNO_2 + h\nu \rightarrow NO_2 + Cl \quad \text{(R6)}$$

This reaction increases the morning abundance of O_x, leading to greater net photochemical O_3 production throughout the day. The other photo fragment, the Cl atom, is highly reactive

towards hydrocarbons and will initiate radical chain reactions that produce O_3 and secondary aerosol (Behnke et al., 1997; Young et al., 2014). The fate and impact of $ClNO_2$ is thus similar to that of nitrous acid (HONO), which also accumulates during the night and photodissociates in the morning to release NO and the hydroxyl radical (OH) that go on to produce O_3 (Alicke et al., 2003).

Data collected during the 2006 Texas Air Quality Study – Gulf of Mexico Atmospheric Composition and Climate Study (TEXAQS-GOMACCS) have shown that $ClNO_2$ production is efficient in the nocturnal polluted marine boundary layer even on primarily non-sea salt aerosol surfaces (Osthoff et al., 2008). As a result, up to 15% of total odd nitrogen (NO_y) was present in the form $ClNO_2$ at night (Osthoff et al., 2008). The high efficiency of $ClNO_2$ formation on aerosol of medium-to-low total chloride content has been confirmed by several laboratory investigations (Bertram and Thornton, 2009; Raff et al., 2009; Roberts et al., 2009) and direct measurements of N_2O_5 uptake on ambient particles (Riedel et al., 2012b). Some ambiguity remains as to the detailed mechanism of R5, but there is agreement that acid displacement of HCl from supermicron (predominantly sea salt aerosol) to submicron (predominantly non-sea salt aerosol) is a key step in the efficient production of $ClNO_2$. These results suggested that this chemistry is active anywhere where pollution in the form of NO_x and O_3 comes in contact with marine air, including the LFV.

However, while the yield of $ClNO_2$ in reaction R5 is high in polluted coastal regions, the $ClNO_2$ yield relative to the amount of NO_3 produced via R1 cannot be easily predicted because NO_3 is consumed by reactions with VOCs (R7), e.g., with biogenic VOCs such as isoprene and monoterpenes as well as aldehydes, and dimethyl sulfide (Wayne et al., 1991).

$$NO_3 + VOC \rightarrow \text{products} \qquad \text{(R7)}$$

Previous studies in the LFV have shown high biogenic VOC concentrations (Biesenthal et al., 1997; Gurren et al., 1998; Drewitt et al., 1998) yet there was active nighttime nitrogen oxide chemistry and aerosol chloride present mainly as sea salt derived aerosol in >1 μm diameter aerosol (Anlauf et al., 2006). During the Pacific 2001 study, measurements of the mixing ratios of NO, NO_2, peroxyacetic nitric anhydride ($CH_3C(O)O_2NO_2$, PAN), HONO, HNO_3, and NO_y at three ground sites in the LFV indicated deficits of up to 15% in the nocturnal NO_y budget (Hayden et al., 2004) attributable to unquantified species such as alkyl nitrates, N_2O_5, and $ClNO_2$. McLaren and coworkers quantified mixing ratios of NO_2 and NO_3 by differential optical absorption spectroscopy (DOAS) at the Sumas Eagle Ridge site (~250 m above the

floor of the LFV) as part of Pacific 2001 (McLaren et al., 2004) and off-shore on Saturna Island (Figure 1) in the Strait of Georgia in 2005 (McLaren et al., 2010). The LFV data showed occasional episodes of active nocturnal nitrogen oxide chemistry in the residual layer with N_2O_5 contributing up to 9% of NO_y, while the Saturna Island data showed NO_3 mixing ratios of > 20 parts-per-trillion by volume (10^{-12}, pptv) every night of measurement. McLaren et al. estimated that between 0.3 and 1.9 ppbv of $ClNO_2$ would be produced under these conditions (2010). Efficient formation of $ClNO_2$ would be consistent with the unidentified O_3 precursor proposed by Ainslie and Steyn and is also a plausible explanation for part of the deficit in the NO_y budget observed by Hayden et al. (2004).

Another feature of the LFV are somewhat unusual diurnal profiles arising from the vertical structure in pollutant concentrations. Measurements of O_3 and NO_2 using tethered balloons by Pisano et al. (1997) during Pacific 93 at the Harris Road site (located ~38 km NW of Abbotsford International Airport) revealed a highly stratified boundary layer with a shallow, 50 m deep isothermal surface layer (also called a nocturnal boundary layer, or NBL) and low surface O_3 concentrations at night. Nocturnal loss of surface O_3 is known to occur by several pathways, including dry deposition, titration with NO (R8), and reaction with unsaturated biogenic hydrocarbons (Neu et al., 1994; Kleinman et al., 1994; Trainer et al., 1987; Logan, 1989; Talbot et al., 2005). Titration of O_3 with NO is readily quantified as the concentration of a product of R8, NO_2, can be measured directly and conserves O_x.

$$O_3 + NO \rightarrow O_2 + NO_2 \qquad \text{(R8)}$$

Usually, the major nocturnal sink of O_x is dry deposition of O_3 and NO_2 (Lin et al., 2010).

The balloon data also showed pools of NO_2 and O_3 in a ~100 m deep nocturnal residual layer (NRL) located 200 to 350 m above ground. Following the break-up of the nocturnal layers in the early morning, vertical down-mixing events of O_3 pollution were observed (McKendry et al., 1997). In this process, pollutants are entrained into the growing mixed layer from the NRL, i.e., the growing mixed layer in the hours after sunrise erodes the somewhat deeper NRL, and pollutants are mixed to the surface (Neu et al., 1994; Kleinman et al., 1994).

In this manuscript, we present the first measurements of $ClNO_2$ and N_2O_5 mixing ratios in the LFV. The data were collected at a surface site east of the Abbotsford International Airport (International Air Transport Association (IATA) airport code YXX) located approximately 35 km from the Pacific Ocean from July 20 to August 5, 2012. Auxiliary measurements

169 included NO, NO_2, NO_y, O_3, photolysis frequencies, and non-refractory PM_1 aerosol
170 composition and size distributions. An analysis of nocturnal nitrogen oxide chemistry
171 including the formation of $ClNO_2$ and its potential impact on nocturnal O_3 and NO_2 loss and
172 radical budgets in the LFV are presented.
173

2 Experimental

2.1 Location

The map shown in Figure 1 indicates the location of the study. Ambient air measurements were conducted at the T45 routine monitoring site located to the east YXX at latitude 49.0212 (N) and longitude -122.3267 (W) and ~60 m above sea level (ASL) and ~30 km from the Pacific Ocean. A raspberry field was located immediately to the W between the end of the airport runway and the measurement site. Nearby local sources included agricultural operations (such as poultry farms) and emissions from motor vehicle traffic on secondary roads and highways. YXX is located ~60 km ESE of the Vancouver International Airport (YVR) and the City of Vancouver. Abbotsford is in the heart of the so-called "Lower Mainland", the low-lying region stretching from Pacific Ocean at Vancouver to the NW and the Canada-USA border to the S (north of Bellingham, BLI) to the eastern end of the Fraser Valley with a total population in excess of 2,500,000.

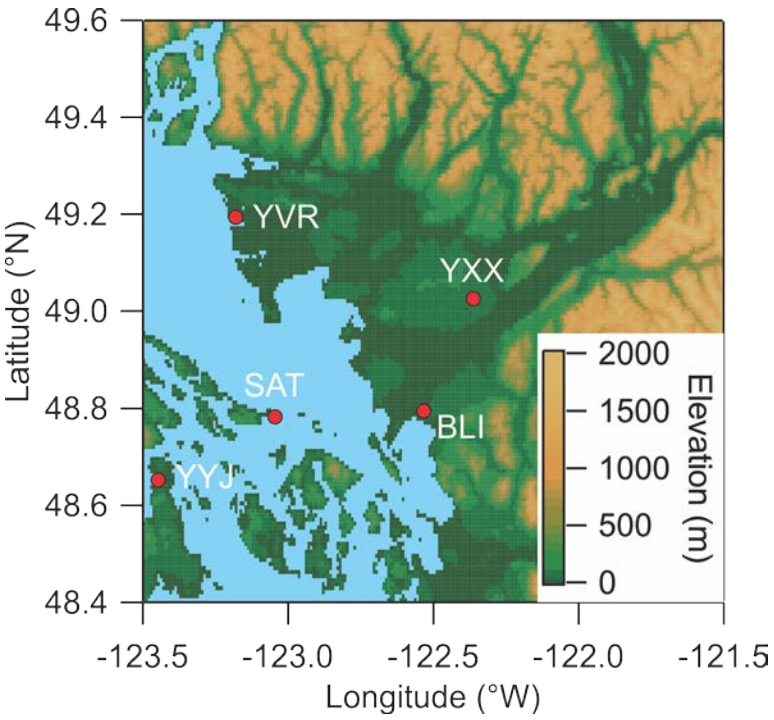

Figure 1. Map of the Lower Fraser Valley. YXX = Abbotsford International Airport (measurement location for this study). YVR = Vancouver Int'l Airport. YYJ = Victoria Int'l Airport. BLI = Bellingham Int'l Airport. SAT = Saturna Island.

2.2 Measurement techniques

The measurement techniques used for this study are listed in Table 1. Data were averaged to 5 min prior to presentation.

The instruments measuring O_3 and nitrogen oxides were housed in an air-conditioned trailer and sampled from a common 0.635 cm (¼") outer diameter (o.d.) and 0.476 cm (3/16") inner diameter (i.d.) Teflon™ inlet at a height of 4 m above ground; the setup is depicted in Figure 3 of Tokarek et al. (2014). A scroll pump whose flow rate was throttled using a 50 standard liters per minute (slpm) capacity mass flow controller was connected to the end of the common inlet to minimize the residence time of the sampled air and to reduce inlet "aging", i.e., accumulation of aerosol on filters of individual instruments, whose inlets tapped into the main inlet line at 90°. The total inlet flow was in the range of 18 to 20 slpm.

Measurements of PM_1 aerosol composition and size distributions (section 2.3) and of meteorological data were made from the research trailer housing the routine measurements at the site. The Agilent VOC measurements were made from a research trailer owned by Environment and Climate Change Canada (ECCC).

2.2.1 Quantification of $ClNO_2$ by iodide chemical ionization mass spectrometry

Mixing ratios of $ClNO_2$ were quantified as iodide cluster ions at *m/z* 208 using the "THS Instruments" iodide chemical ionization mass spectrometer (iCIMS) described by Mielke et al. (2011) and calibrated using the scheme by Thaler et al. (2011). In this method, a gas stream containing $ClNO_2$ is generated from reaction of Cl_2 (Praxair, 10 ppmv in N_2) with an aqueous slurry saturated with $NaNO_2$ (Sigma-Aldrich) (R9):

$$Cl_2(g) + NO_2^-(aq) \rightleftharpoons ClNO_2(g) + Cl^-(aq) \quad \text{(R9)}$$

This gas stream was periodically added to the main inlet with the aid of a normally-open 2-way valve connected to a vacuum pump in a similar fashion as described earlier for N_2O_5 and PAN (Tokarek et al., 2014; Odame-Ankrah and Osthoff, 2011). The $ClNO_2$ content of the calibration gas stream was quantified by thermal dissociation cavity ring-down spectroscopy (TD-CRDS) as described in section 2.2.2. In total, 31 calibrations for $ClNO_2$ were carried out, spread out evenly over the measurement period. The iCIMS response factor at *m/z* 208 was (0.40±0.06) Hz $pptv^{-1}$ (where the error represents the standard deviation of repeated calibrations), normalized to 10^6 counts of reagent ion at *m/z* 127. The $^{37}ClNO_2I^-$ ion at *m/z* 210

was also monitored and found to be (0.298±0.004) times the signal at *m/z* 208 (r^2 = 0.944), slightly lower than Standard Mean Ocean Chloride ^{37}Cl mole fraction in sea water of ~0.319 (Wieser and Berglund, 2009) and our previously observed ratios of 0.315±0.003 in Calgary (Mielke et al., 2011) and 0.3065±0.0002 in Pasadena (Mielke et al., 2013). The reason(s) for these differences are unclear but may be a result of fractionation processes (Koehler and Wassenaar, 2010; Volpe et al., 1998), a topic outside the scope of this manuscript.

The iCIMS was also used to quantify mixing ratios of PAN at *m/z* 59 and PPN at *m/z* 73 (Slusher et al., 2004; Mielke et al., 2011; Mielke and Osthoff, 2012). For this reason, part of the instrument's inlet prior to the ion-molecule reaction region was heated to 190 °C to dissociate PANs into their respective carboxylates. Further, the collisional dissociation chamber (CDC) was operated in declustering mode (-22.7 V) to break up ion clusters. Calibrations and matrix effect correction procedures and a time series of the PAN and PPN data were presented by *Tokarek et al.* (2014).

2.2.2 Quantification of NO_2 and N_2O_5 by cavity ring-down spectroscopy

The CRDS used in this work was an amalgamated version of two instruments described earlier (Paul and Osthoff, 2010; Odame-Ankrah and Osthoff, 2011), called "Improved Detection Instrument for Nitrogen Oxide Species" (iDinos) (Odame-Ankrah, 2015). A schematic of the optical layout is shown in Figure 2. The optical bread board, instrument frame, electronic and data acquisition components were as described by *Paul and Osthoff* (2010). The new instrument was set up with up to six parallel detection channels: four 405 nm "blue" diode laser CRDS cells for quantification at NO_2 via its absorption at 405 nm with a distance between the pairs of high-reflectivity (HR) mirrors (Advanced Thin Films) of 112.5 cm, of which 92.0 cm were filled with sample air, and two newly constructed 662 nm "red" diode laser CRDS cells for quantification at NO_3 via its absorption at 662 nm with a distance between the HR mirrors (Los Gatos) of 93.0 cm of which 73.0 cm were filled with sample air. Light exiting the far ends of the CRDS cells was collected using fixed-focus collimating lenses and multimode optical fibers (Thorlabs) connected to photomultiplier tubes (PMT, Hamamatsu H9433-03MOD) with 10 MHz bandwidth. Bandpass filters (Thorlabs FB405-10 and FB660-10) were placed between the PMTs and the end of the optical fibers.

The two laser diodes were simultaneously square-wave modulated by a function generator (SRS DS335). The PMT voltages were digitized using an 8-channel 14-bit data acquisition

card (National Instruments PCI-6133; 2.5 MS s^{-1} simultaneous sampling sample rate) connected to a laptop computer via a PCMCIA-to-PCI expansion unit (Magma CB4DRQ) and controlled by software written in LABVIEW™ (National Instruments).

Ring-down time constants (τ) were determined from a linear fit to the logarithm of the digitized PMT voltage as described by *Brown et al.* (2002) immediately after acquisition of the ring-down traces (which were co-added to a user-selectable averaging time prior to the fit). The fitting algorithm requires the subtraction of the PMT voltage offset prior to taking the logarithm; this offset was measured between ring-down events after the signal had returned to baseline, which limited the repetition rate of the diode lasers and the number of traces averaged per second to a frequency of 300 Hz.

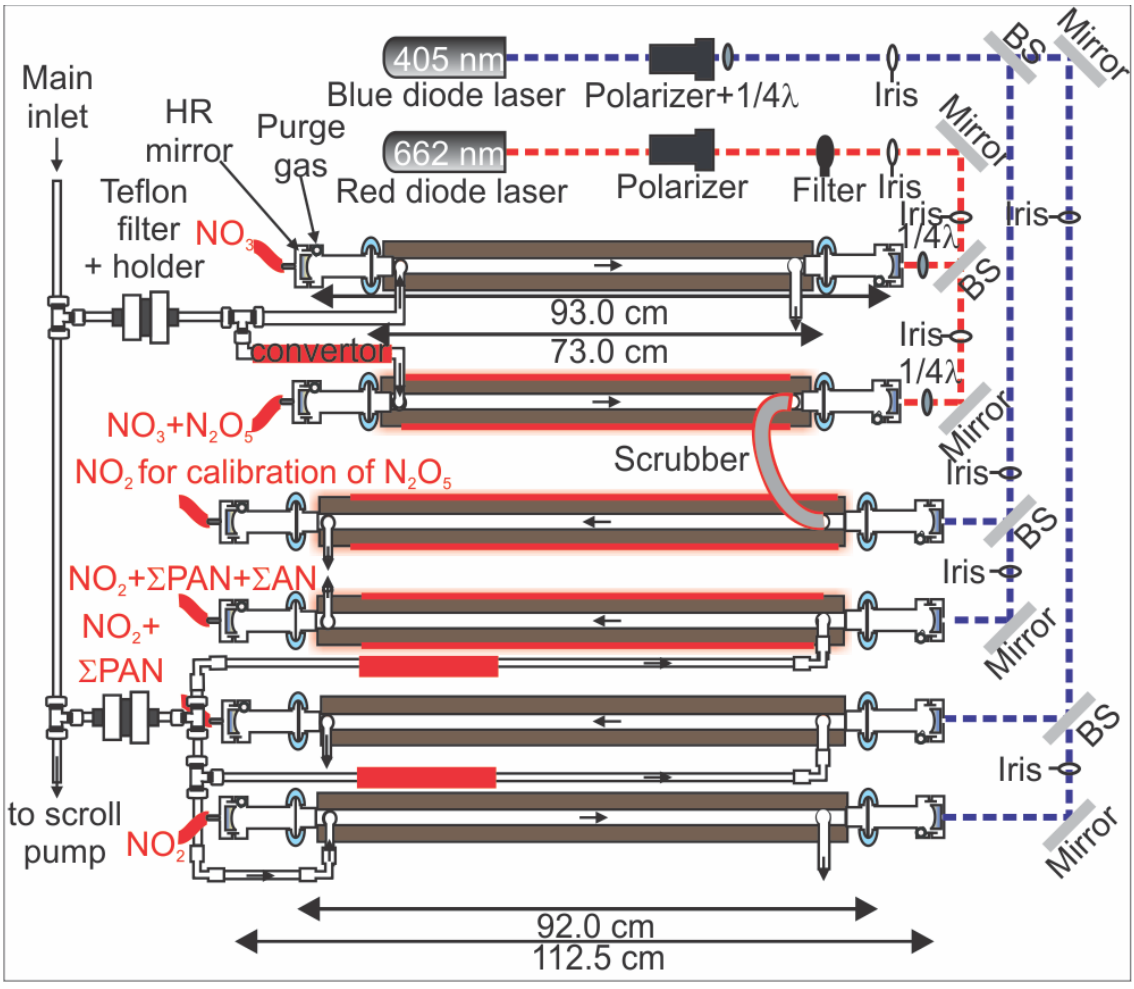

Figure 2. Optical layout of the cavity ring-down spectrometer. ¼λ = quarter wave plate. BS = beam splitter. HR mirror = high reflectivity mirror. Drawing is not to scale.

Ring-down time constants in the absence of the target absorber (τ_0) were determined by flooding the inlet (each once per hour) with ultra-pure, or "zero", air (Praxair) for the 405 nm channels and by titration with NO for the 662 nm channel (Brown et al., 2001; Simpson, 2003) Typical values of τ_0 were in the range of 63 to 67 μs and between 198 and 210 μs for the blue and red channels, respectively. The baseline precision (i.e., standard deviation, σ) of the NO_2 and NO_3 measurements were ±80 pptv and ±3 pptv (1 s data), respectively. For the NO_3 channels, additional noise was introduced by variable background absorption of NO_2, O_3, and water vapor which produce small, spurious structure in the 662 nm absorption signal (Dubé et al., 2006) and were not tracked well by the interpolation of the baseline from the hourly τ_0 determinations.

During the Abbotsford campaign, only five (four blue and one red) CRDS channels were operated because of delays in the fabrication of the final set of CRDS mirror holders. The 662 nm CRDS cell sampled from a Teflon™ inlet heated to 130 °C for quantification of NO_3 plus the NO_3 generated from thermal dissociation N_2O_5 (Brown et al., 2001; Simpson, 2003; Dubé et al., 2006). Under the high-NO_x conditions of this study, equilibrium (2) was sufficiently far to the right (see section 3.3) such that $[NO_3] + [N_2O_5] \approx [N_2O_5]$, i.e., the concentration measured could be equated with $[N_2O_5]$ without introducing a large error (i.e., <5%). The four 405 nm CRDS cells were operated as follows: The first sampled from an ambient temperature inlet and was used to quantify NO_2. The second sampled from a quartz inlet heated to 250 °C and was used to quantify NO_2 plus total peroxyacyl nitrate (ΣPAN) (Paul et al., 2009; Paul and Osthoff, 2010). Data from this channel will be presented in a future manuscript. The third was operated with a quartz inlet heated to 450 °C to enable $ClNO_2$ calibrations (Thaler et al., 2011). Quantification of total alkyl nitrates (ΣAN) in ambient air was not attempted because of the high NO_x levels and resulting large subtraction errors (Thieser et al., 2016). The fourth 405 nm CRDS cell was connected with polycarbonate tubing (⅜" o.d. and ¼" i.d.) in series to the 662 nm channel and was used to calibrate the response of the N_2O_5 channel, which is a function of the transmission efficiency of N_2O_5 through the inlet and the overlap of the diode laser spectrum with the NO_3 absorption line (Odame-Ankrah and Osthoff, 2011). The role of the polycarbonate tube was to scrub NO_3 exiting the N_2O_5 channel, allowing detection of only the NO_2 generated from thermal

dissociation of N_2O_5 and to prevent recombination of NO_3 and NO_2 in the blue calibration channel (Wagner et al., 2011).

N_2O_5 was generated in situ by adding an excess of O_3 (generated by passing O_2 past a 254 nm Hg lamp) to nitric oxide (NO) in a 0.635 cm (¼") o.d. and 0.476 cm (3/16") i.d. Teflon™ calibration line and allowed to equilibrate (i.e., until the output was constant) offline before being switched inline on demand. The N_2O_5 response (which accounted for N_2O_5 loss in the sampling line and slight mismatches of the laser wavelengths with the NO_3 absorption line) varied between 65% and 100% and depended on inlet "age"; the Teflon™ inlet and aerosol inlet filter were changed every 2 – 3 days. The accuracy of the NO_2 and N_2O_5 data were ±10% and ±25%, respectively, driven mainly by the systematic uncertainty of the NO_2 absorption cross-section and of the N_2O_5 inlet transmission efficiency (Odame-Ankrah, 2015).

2.2.3 Measurements of O_3, NO and NO_y,

Mixing ratios of O_3 were monitored by UV absorption in a commercial instrument (Thermo 49) and were accurate within ±2% and ±1 ppbv. An NO-O_3 chemiluminescence instrument (Thermo 42i) was used to monitor mixing ratios of NO and NO_y, which was reduced to NO in a Mo converter heated to ~320 °C placed outside a short distance (~ 1 m) from the sample inlet. This instrument sampled from the main inlet via a Teflon™ filter and filter holder and was calibrated daily against CRDS as described by Tokarek et al. (2014). The slope uncertainty for each multipoint calibration was ±15%. Interpolation between calibration runs gave an overall uncertainty of ±30%. The NO zero offset uncertainty (needed for calculating the NO_3 loss rate with respect to reaction with NO, R9) was ±10 pptv.

2.2.4 VOC measurements

Volatile organic compounds were monitored with a commercial gas chromatograph - mass spectrometer (GC-MS; Agilent model 7890A and 5975C) equipped with an FID detector and a Markes Unity 2 pre-concentrator with an ozone precursor trap cooled to -25 °C.

In a typical sampling sequence, a 500 mL air sample was collected at a flow rate of 25 mL min^{-1}, taken from the center flow of a 1.27 cm (½") stainless steel inlet line which was continuously sampling ambient air at 5 L min^{-1}. The sampled air flowed through a 0.318 cm

(1/8") stainless steel line and particles were removed using a 1 µm pore size fritted filter. Once 500 mL of air were collected, the pre-concentrator was flushed with helium to remove air while awaiting injection. At the start of a GC run, the sample in the pre-concentrator was flash heated to 300 °C and held for 3 min. The sample was separated on 2 columns with the entire sample going through the Agilent VRX column with a Dean switch directing the first gases emitted to a second GasPro column and then to the FID detector (~<C4) while the heavier compounds were detected using the MS detector in scan mode.

The cycle time for the GC analysis was 1 hour with the sample being collected during the previous runs analyses. The 20 min sample was taken at the start of a 1 hour time period.

Due to the low temperature of the trap, the air was dried using a trap at -30 °C. The trap was heated and dried between each sample and reconditioned for 10 min prior to sample collection. All sample lines were stainless steel with a Restek Sulfinert^{TM} coating to minimize sample loss on the lines. Calibrations were performed once per day for 105 species using a 100 ppbv U.S. Environmental Protection Agency (EPA) photochemical assessment monitoring system (PAMS) and a 100 ppb EPA air method, toxic organics – 15 (TO15) standard tanks (Linde Specialty Gases) at an approximately concentration of 2 ppbv. The terpenes were semi-quantitatively measured as a calibration source was not available at the time and only the changes in concentration strength with time of day were used. The accuracy of the measurements varied depending on the species but was better than ±30% throughout. Peaks were manually reintegrated using Chemstation software from Agilent. Table S-1 summarizes the VOCs quantified.

2.3 Aerosol measurements

The chemical composition of non-refractory PM_1 was monitored using an Aerosol Chemical Speciation Monitor (ACSM, Aerodyne), which reported concentrations of NO_3-, SO_4^{2-}, Cl^-, NH_4^+, and total organics. A general description of this instrument designed for routine monitoring has been given by Ng et al. (2011). The composition of the refractory aerosol (i.e., sea salt) was not quantified.

Submicron aerosol size distributions were quantified by a scanning mobility particle sizer (SMPS, TSI 3034). This instrument measured aerosol particles in the range from 10 to 487 nm using 54 size channels (32 channels per decade). Both of these instruments were housed in

a trailer operated by Metro Vancouver. The ACSM and the SMPS sampled air off a shared stainless steel inlet that had a total flow of 5 L min^{-1} and contained a $PM_{2.5}$ sharpcut filter at the inlet and was operated at ambient relative humidity.

2.4 Photolysis frequencies

Photolysis frequencies were determined by solar actinic flux spectroradiometry (Hofzumahaus et al., 1999) using a commercial radiometer with 2π receptor optics and photo diode array (PDA) detector (Metcon; 512 pixels, wavelength range 285 nm - 690 nm) calibrated by the manufacturer. The spectrometer was mounted facing up (zenith view) and hence measured the down-welling radiation. On several days, the spectrometer was inverted hourly to determine the up-welling radiation, which was added to the down-welling flux. Photolysis frequencies including $j(NO_3)$, $j(NO_2)$, $j(O^1D)$, and $j(ClNO_2)$ were calculated using reference spectra and quantum yields from (Sander et al., 2010) and (Ghosh et al., 2012). Table 2 gives the ratio of observed up-welling to down-welling for selected photolysis frequencies. For August 3 (a cloud-free day), the measurements were compared to (hourly) predictions with the online "Tropospheric Ultraviolet and Visible (TUV) Radiation Model" V5.0 (Madronich and Flocke, 1997); with default settings, the model reproduced the measured $j(NO_2)$ and $j(O^1D)$ quite well: a scatter plot of observed against TUV rate constants had correlation coefficients (r) of 0.997 and 0.998, slopes of 1.06±0.02 and 1.10±0.02, and offsets of $(3\pm1)\times10^{-4}$ s^{-1} and $(5\pm3)\times10^{-7}$ s^{-1}.

2.5 Box model simulations of the nocturnal O_3 and O_x loss in the NBL

A box model was set up to reconcile the median nocturnal decays of O_3 and O_x. These simulations are intended as back-of-the-envelope type estimates of major processes only since an accurate description of the nocturnal boundary layer chemistry would require modeling of horizontal and vertical transport, i.e., altitude-resolved information not available in this study (Geyer and Stutz, 2004). The model's assumptions are a well-mixed NBL that is decoupled from the NRL above it as observed by earlier balloon vertical profiling (Pisano et al., 1997), O_3 and NO_2 dry deposition velocities of $v_d(O_3)$ = 0.2 cm s^{-1} and $v_d(NO_2) = \alpha \times v_d(O_3)$ with α=0.65 (Lin et al., 2010), and negligible chemical O_3 and O_x losses other than titration of O_3 by NO (R8) and by reaction with a generic biogenic hydrocarbon (assumed to react with O_3

with a rate coefficient of 5×10^{-11} cm^3 $molec.^{-1}$ s^{-1}, i.e., the rate coefficient for reaction of α-pinene with O_3 (Seinfeld and Pandis, 2006)). Simulations were initiated with the median NO_2 and O_3 concentrations observed at sunset. More details are given in the S.I.

3 Results

3.1 Overview of data set

3.1.1 Meteorology

A time series of local wind direction and speed are displayed in Figure 3D. During the two-week long measurement period, the air flow to the site was from the Pacific Ocean to the SW and WSW with a moderate wind speed of 8.7 km hr^{-1} (median value). On most nights, local wind speeds were calm, i.e., < 5 km hr^{-1} (median speed 3.6 km hr^{-1}) and from variable directions, though predominantly from the W and N. The two exceptions were the nights of July 22/23 and August 1/2 when stronger winds (> 5 km hr^{-1}) from the W and SW persisted. These nights saw relatively high $ClNO_2$ mixing ratios (see section 3.1.4).

The air temperatures were quite mild and ranged from a minimum of 11.0 °C to a maximum of 31.9 °C. The warm temperatures shifted equilibrium K_2 from N_2O_5 towards NO_3 and NO_2 (further analyzed in section 3.2.2). At night, temperatures frequently dropped to the dew point, resulting in occasional fog formation (shown as grey rectangles in Figure 3D), sometimes after sunrise. Fog droplets are strong sinks for N_2O_5 (Osthoff et al., 2006). In total, the impact of fog was minor, affecting 5% of the data. In addition, there were two periods with precipitation: The first occurred intermittently on July 20 until the morning of July 21. The second rainfall event was a 24-hour period from mid-day July 22 to the afternoon of July 23 (shown as blue dots in Figure 3D). July 23 also exhibited the highest wind speeds of the campaign (Figure 3C) and lowest daytime photolysis frequencies. The time series of $j(ClNO_2)$ is shown as a representative example in Figure 3A. The photolysis data indicates that it was sunny on 6 days (July 25, 26, 29, Aug 1, 4 and 5) and that the remaining days had variable cloud cover, consistent with hourly meteorological logs that showed 10% of the measurement period affected by precipitation.

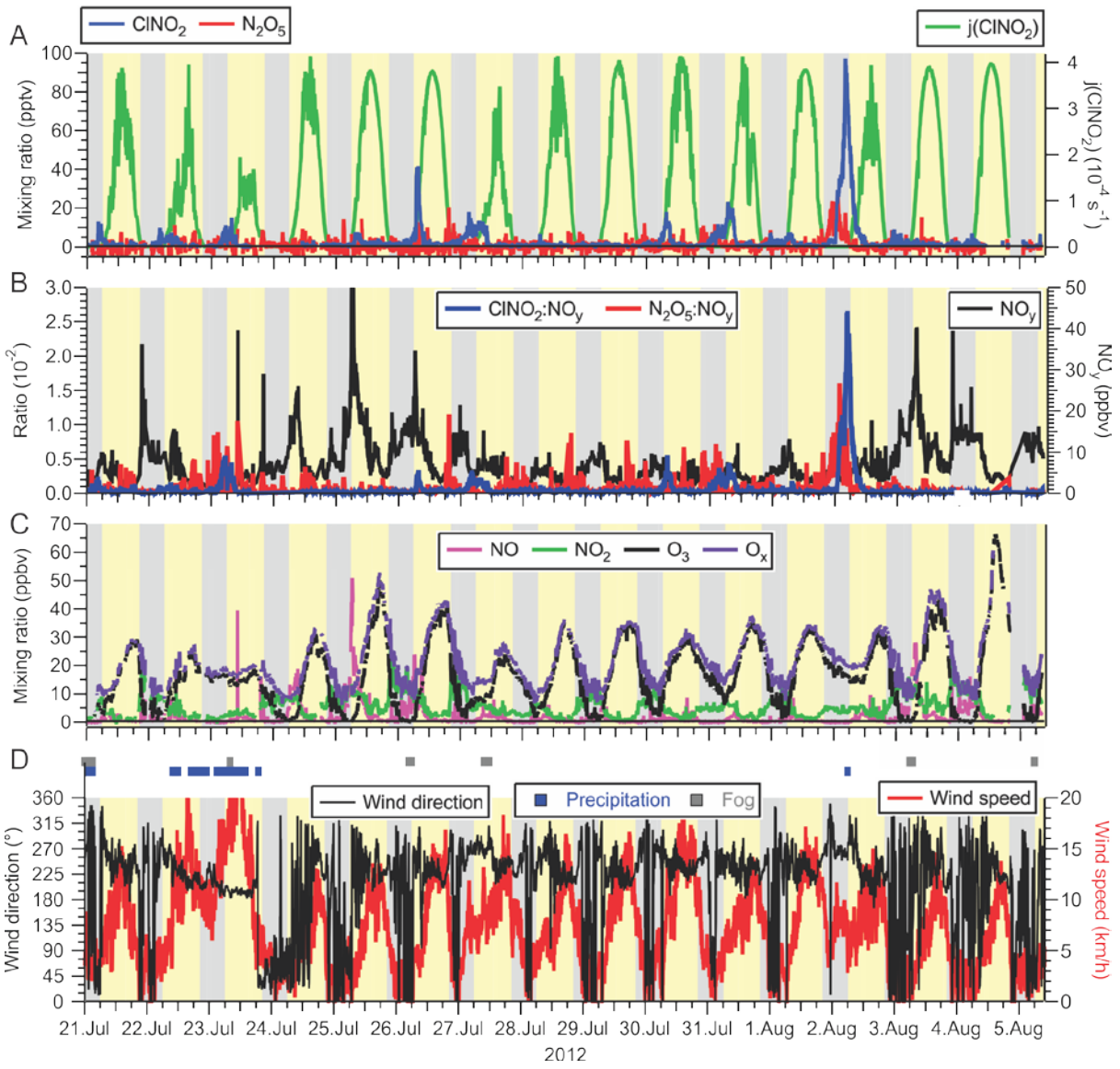

Figure 3. (**A**) Time series of N_2O_5 and $ClNO_2$ mixing ratios (left axis) and $ClNO_2$ photolysis frequency (right axis) observed at T45 near the Abbotsford International Airport. (**B**) Time series of the ratios of $ClNO_2$ and N_2O_5 to NO_y (left axis) and of NO_y (right axis). (**C**) Time series of NO, NO_2, O_3, and O_x (= NO_2 + O_3) mixing ratios. (**D**) Time series of local wind direction (left axis) and speed (right axis). The blue and grey dots above the time series indicates periods of precipitation (drizzle or rain) and fog, respectively, as identified in hourly meteorological logs.

3.1.2 NO and NO_2

The rates of N_2O_5 and $ClNO_2$ formation depend on the rate of NO_3 production, $P(NO_3)=k_1[NO_2][O_3]$ (analyzed further in section 3.2.2); therefore, it is informative to first examine the mixing ratios of NO_2 and O_3 (see section 3.1.3). The time series of NO, NO_2, O_3, and O_x (= O_3 + NO_2) mixing ratios are shown in Figure 3C, and their diurnal averages are shown as 10^{th}, 25^{th}, 50^{th}, 75^{th} and 90^{th} percentiles in Figures 4B and 4C.

The median NO and NO_2 mixing ratios for the entire campaign were 0.9 and 5.9 ppbv, respectively. The average NO_x/NO_y ratio for the entire campaign was 0.9±0.4. These concentration levels are characteristic of an urban air mass impacted by relatively fresh emissions from combustion engines in automobiles.

At night, mixing ratios of NO were generally lower than during the day though not negligible (median 0.3 ppbv, Figure 4B) as NO was oxidized by O_3 to NO_2 (R8) and was not replenished by NO_2 photolysis. However, mixing ratios of NO increased throughout the night, often coinciding with complete nocturnal removal of O_3 (see section 3.1.3), which indicates the presence of nearby combustion sources of NO_x (most likely automobile exhaust). The presence of NO titrates NO_3 (R3) and effectively shut down N_2O_5 and $ClNO_2$ production for most of the study: 68% of the measurement period had NO mixing ratios > 100 pptv and NO_3 lifetimes (with respect to its reaction with NO) of < 15 s. In contrast, NO_2 mixing ratios were highest at night (median 7.3 ppbv), amplified further by NO_x emissions that continued throughout the night and likely by low nocturnal mixing heights (see discussion).

Mixing ratios of NO and NO_x were highest in the morning hours. Concentration changes at this time of day are difficult to interpret since the NBL breaks up during this time, resulting in vertical mixing of air masses, photolabile species (e.g., $ClNO_2$, HONO, N_2O_5, etc.) that accumulated overnight begin to photodissociate, and local emissions change with the onset of rush hour.

In contrast to the morning increase in NO, an afternoon/early evening maximum in NO was absent. This can be rationalized by a greater abundance of oxidants that oxidize NO to NO_2, i.e., O_3 (see Figures 3 and 4 and section 3.1.3) and organic peroxy radicals in the afternoon, a topic outside the scope of this manuscript.

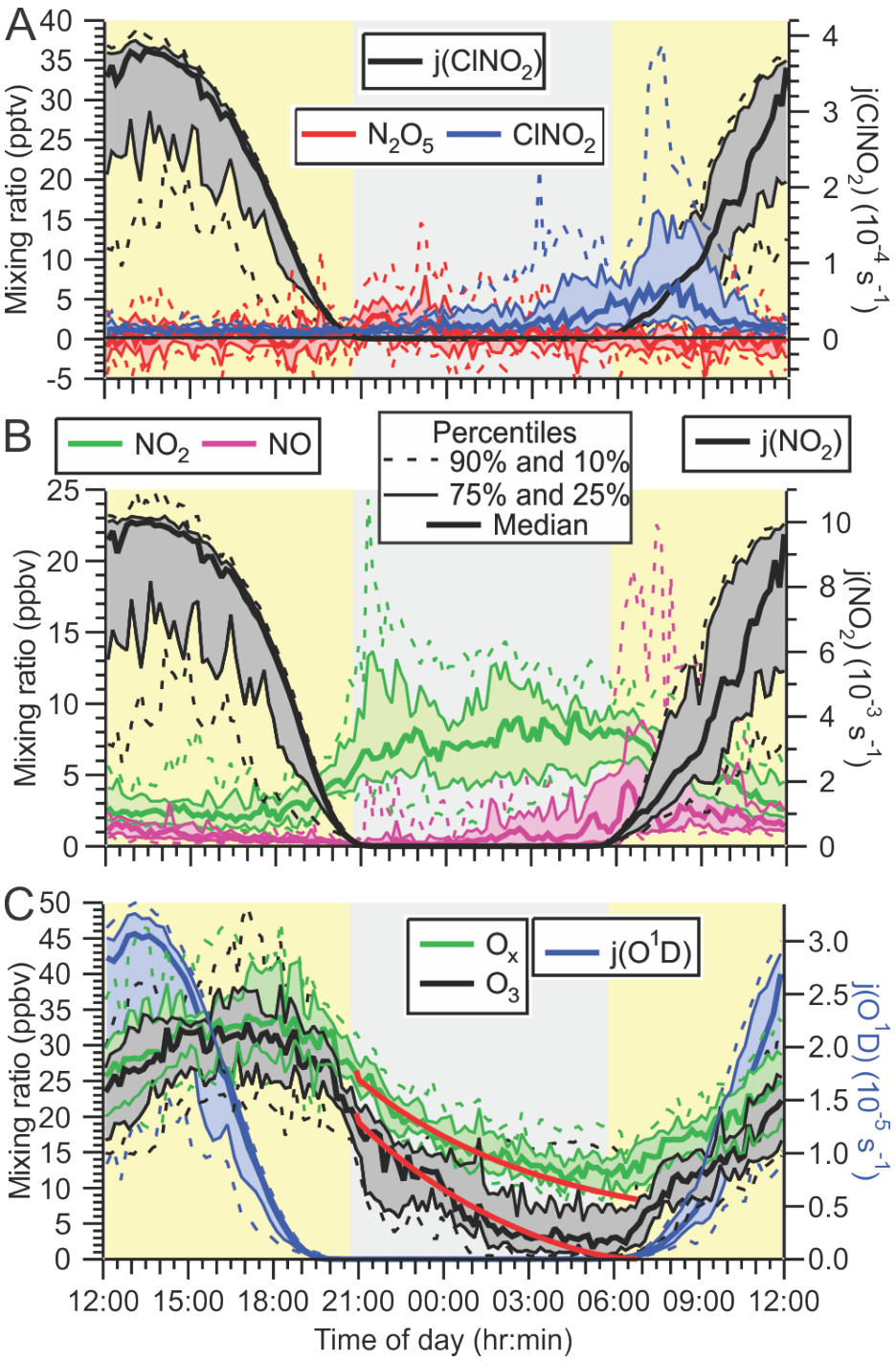

Figure 4. (**A**) Diurnal variation of $ClNO_2$ and N_2O_5 mixing ratios (left axis) and $ClNO_2$ photolysis frequencies (right axis). (**B**) Diurnal profiles of NO and NO_2 (left axis) and NO_2 photolysis frequency (right axis). (**C**) Diurnal profiles of O_3 and $O_x = O_3 + NO_2$ (left axis) and $O_3 \rightarrow O(^1D)$ photolysis frequency (right axis). The superimposed lines shown in red are results from a simple box model (see text).

3.1.3 O_3 and O_x

The time series of O_3 mixing ratios and its diurnal profile are shown in Figure 3C and 4C, respectively. O_3 mixing ratios were small (average ± 1 standard deviation of 16±12 ppbv) and peaked at ~17:00 in the afternoon. The highest concentrations were observed on August 4 from 13:55 to 15:30, when mixing ratios were 64±1 ppbv (the 8-hour running average was 52 ppbv). These levels were well below the CAAQS 8-hr standard of 63 ppbv and the 1 hour National Ambient Air Quality Objective of 82 ppbv, smaller than the pre-2003 data analyzed by Ainslie and Steyn (2007), who reported between 10 and 20 O_3 1-hour exceedences of 82 ppbv in the 1980s, and of similar magnitude as observed by a high-density monitoring network in the region in 2012 (Bart et al., 2014), which observed peak O_3 levels of 74 and 83 ppbv at Abbotsford on July 8 and August 17, respectively.

A recurring feature of this data set was the rapid and often complete loss of O_3 at night (Figure 4C). This was accompanied by an increase in the NO_2 mixing ratios, though by less (+6 ppbv on average) than the amount of O_3 that was lost (-26 ppbv on average), showing that NO to NO_2 conversion (R8) was a contributor, though minor (~25%) to the nocturnal O_3 loss.

The diurnal profile of O_x was similar to that of O_3, in that the highest concentrations occurred in the afternoon (at ~18:00) and a considerable fraction of O_x was removed at night. At sunset, a median amount of 26 ppbv of O_x were present, which decreased to 12 ppbv at sunrise (Figure 4C). The pathways contributing to nocturnal O_3 and O_x loss are probed using box model simulations in section 3.2.1.

There were two (out of 16 total) nights when O_3 was not completely removed. On July 22-23 and August 1-2, O_3 mixing ratios dropped from a daytime maxima of ~33 ppbv to non-zero nocturnal minima of ~16 ppbv. On both of these nights, $ClNO_2$ and N_2O_5 mixing ratios were elevated (Figure 3A), and the two largest $ClNO_2$ to NO_y ratios were observed (Figure 3B). The local wind speeds were > 6 km hr^{-1}, whereas on other nights, local winds were calmer (Figure 3C). The greater local wind speeds likely induced more turbulence and a higher vertical mixing height.

3.1.4 N_2O_5 and $ClNO_2$

Time series of $ClNO_2$ and N_2O_5 mixing ratios and $ClNO_2$ photolysis frequencies are shown in Figure 3A. Mixing ratios of $ClNO_2$ and N_2O_5 were small (campaign averages at night of 4.0 pptv and 1.4 pptv, respectively). The mixing ratios peaked prior to sunrise at median values of 7.9 and 7.8 pptv for $ClNO_2$ and N_2O_5, respectively. The highest mixing ratios of this campaign were 97 pptv for $ClNO_2$ and 23 pptv for N_2O_5, both observed on the night of August 1-2. This night was also the only time when nocturnal $ClNO_2$ mixing ratios exceeded 20 pptv and is analyzed in greater detail in section 3.2.3.

Consistent with their low mixing ratios, neither $ClNO_2$ nor N_2O_5 were significant components of NO_y (Figure 3B): on average, they contributed 0.1% to the nocturnal NO_y budget, though NO_y mixing ratios were large (median 6.3 ppbv at night), typical for a site impacted by urban emissions. The only exception was the night of August 1-2, when $ClNO_2$ and N_2O_5 constituted 2.6% and 1.6% of NO_y, respectively, and NO_y mixing ratios were 4.4 ppbv on average (Figure 3B).

The $ClNO_2$ and N_2O_5 mixing ratios are displayed as functions of time of day in Figure 4A. Before midnight local time, N_2O_5 mixing ratios were slightly larger (median value of 1.8 pptv on average) than those of $ClNO_2$ (median value of 1.4 pptv on average), whereas after midnight, $ClNO_2$ mixing ratios were larger than those of N_2O_5 (2.0 pptv vs. 0.6 pptv). The latter is consistent with observations at other ground sites, which generally showed higher concentrations of the longer-lived $ClNO_2$ prior to sunset (Thornton et al., 2010; Mielke et al., 2013). The higher N_2O_5 than $ClNO_2$ abundances at the beginning of the nights suggests that the N_2O_5 production rate at that time exceeded its ability to react heterogeneously and convert to $ClNO_2$, potentially due to a lack of available aerosol chloride or otherwise reduced N_2O_5 heterogeneous uptake parameters (Thornton et al., 2010).

Production of $ClNO_2$ from N_2O_5 uptake on aerosol ceases after sunrise because of the rapid removal of N_2O_5 and NO_3 as the latter is titrated by NO and destroyed by photolysis (R3 and R4) (Wayne et al., 1991). In spite of this, $ClNO_2$ mixing ratios frequently (on 12 out of 15 measurement days) continued to increase after sunrise (Figures 3A and 4), peaking on average at ~07:45 in the morning approximately 2 hours after sunrise. The median mixing ratio at that time was 6.7 pptv larger than the median value of 5.3 pptv observed at sunrise. The most prominent example of this phenomenon occurred on the morning of July 26. For a two hour period leading up to sunrise, there was fog (virtually ensuring the absence of N_2O_5), and

$ClNO_2$ mixing ratios were < 5 pptv. The fog then dissipated at sunrise. One hour later, $ClNO_2$ mixing ratios increased to > 40 pptv. Similar events (though with more modest $ClNO_2$ increases) were observed on the mornings of July 22, 23, 25, 27, 28, 30, 31, and Aug 1. Two of these (July 23 and 27) overlapped with brief fog events.

Qualitatively similar $ClNO_2$ morning peaks have been observed at other ground sites and were rationalized by vertical mixing (Tham et al., 2016; Bannan et al., 2015; Faxon et al., 2015).

In the period after the $ClNO_2$ morning peak after ~09:00, $ClNO_2$ mixing ratios decreased, coinciding with the increasing $ClNO_2$ photolysis rate. Box model simulations (see S.I.) indicate that the decay of $ClNO_2$ (after 09:00) was consistent with its destruction by photolysis.

There were two exceptions: the mornings of July 27 and Aug 2, when the decay of $ClNO_2$ concentration occurred at a rate faster than its photolysis. On July 27, fog was not observed until 8:00, at which time the $ClNO_2$ mixing ratio rapidly decreased because of dissolution and/or an air mass shift to one with a different chemical history. On Aug 2, the campaign maximum of 97 pptv was observed at 04:40 prior to sunrise, followed by a sharp decline. Hourly logs indicated scattered showers at 06:00.

3.1.5 PM_1 size distribution and composition measurements

The time series of PM_1 surface area density (S_A) observed by the SMPS is shown in Figure 5A. The aerosol loadings were modest: the average (median) surface area density was 128 (104) $\mu m^2\ cm^{-3}$ and ranged from extremes of 26 to 618 $\mu m^2\ cm^{-3}$. The size distribution data show that bulk of the surface area (i.e., the mean diameter ($\bar{D}_s$)) is in the range of 200 to 300 nm, such that most of the area of the accumulation mode was captured. However, the surface area calculations do not include contributions from larger diameter particles which were not quantified. Shown on the right hand side of Figure 5A is the rate coefficient for heterogeneous uptake of N_2O_5, $k_{N_2O_5}$ calculated using equation (1).

$$k_{N_2O_5} = \frac{1}{4}\gamma \bar{c} S_A \quad (1)$$

Here, γ and $\bar{c}$ are the uptake probability and the mean molecular speed of N_2O_5, respectively. Equation (1) is valid for uptake on small, submicron aerosol as it neglects gas-phase diffusion

limitations (Davidovits et al., 2006). For this calculation, a γ value of 0.025 was assumed. The average ($\pm$1 standard deviation) of $k_{N_2O_5}$ was $(2\pm1)\times10^{-4}$ s^{-1}.

The ACSM submicron aerosol composition data are shown as a time series in Figure 5B and as a function of time of day in Figure 6. Consistent with the size distributions, mass loadings were also modest overall (average 2.3 μg m^{-3}). The ACSM factor analysis identified oxygenated organic aerosol (OOA) as the largest mass fraction of the non-refractory aerosol (average ± standard deviation 1.4±1.2 μg m^{-3}, 63.3% of the total aerosol mass measured by the ACSM). Hydrocarbon-like organic aerosol (HOA) associated with primary emissions was a minor component (average 0.03 μg m^{-3}, 1.1%) but occasionally enhanced in plumes (maximum 8.3 μg m^{-3}). The oxygenated aerosol fraction (OOA) did not exhibit a discernible diurnal profile (Figure 6A), which is consistent with the modest photochemistry at this site as judged from the modest peak O_3 levels observed. The inorganic mass fraction was dominated by nitrate (0.47±0.40 μg m^{-3}, 20.7%). The second most abundant inorganic component was ammonium (0.2±1.4 μg m^{-3}, (8.8%) followed by sulfate (0.15±0.15 μg m^{-3}, 6.8%). The data are of similar magnitude as aerosol mass spectrometry (AMS) data collected at nearby Langley as part of Pacific 2001 (Boudries et al., 2004); then, organics had also been the largest component (average of 1.6 μg m^{-3}, 49%), though sulfate and ammonium mass loadings had been larger (0.88 and 0.44 μg m^{-3}, 25% and 14%, respectively) and nitrate mass loadings smaller (0.38 μg m^{-3}, 12%).

The neutralization ratio, NR $\approx$ $[NH_4^+]$:($[NO_3^-]$+2$[SO_4^{2-}]$) (Zhang et al., 2007), where the square brackets denote molar concentrations (calculated from the mass concentrations reported by the ACSM by dividing by the appropriate molecular weights), was 1.19 (median value). The high NH_3 content is qualitatively consistent with the non-quantitative data collected by Metro Vancouver (using a Thermo Scientific 17i NH_3/NO/NO_2/NO_x analyzer), which showed large concentrations of gas-phase NH_3 (Figure S-1).

The ACSM software also reported non-refractory chloride with an average ($\pm$1 standard deviation) concentration of 0.01±0.03 μg m^{-3}, though it is unclear if this signal was real as it did not vary over the course of the campaign and was below the stated ACSM detection of limit of 0.2 μg m^{-3} (Ng et al., 2011).

Aerosol nitrate exhibited a clear diurnal profile with higher concentrations at night (Figure 6B). In particular, the amount of aerosol nitrate increased at the beginning of the night, when the nocturnal NO_3 production rates were greatest.

589 Previous AMS measurements in Vancouver during the month of August as part of Pacific
590 2001 reported a slightly higher total mass loadings of 7.0 μg m^{-3} that included a greater HOA
591 component (2.4 μg m^{-3}, 34%) and a smaller nitrate fraction (0.6 μg m^{-3}, 8.5%) (Alfarra et al.,
592 2004; Jimenez et al., 2009) than observed here. The lower HOA in this data set are likely a
593 result of tighter emission controls implemented since the earlier study, a topic outside the
594 scope of this paper.
595

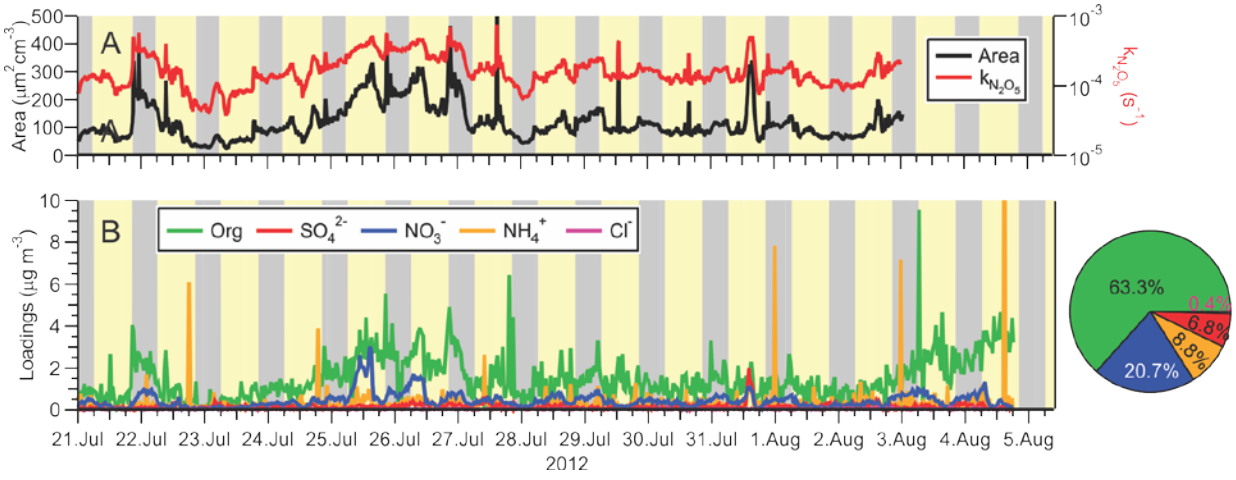

596

597 **Figure 5**. Time series of (A) submicron surface area density measured by the TSI 3034
598 scanning mobility particle sizer (left-hand side) and calculate heterogeneous N_2O_5 uptake rate
599 coefficient assuming γ=0.025 (right-hand side), and (B) non-refractory submicron aerosol
600 species measured by ACSM. The average total loading was 2.3 μg m^{-3}. The pie chart shows
601 the average campaign composition.
602

603

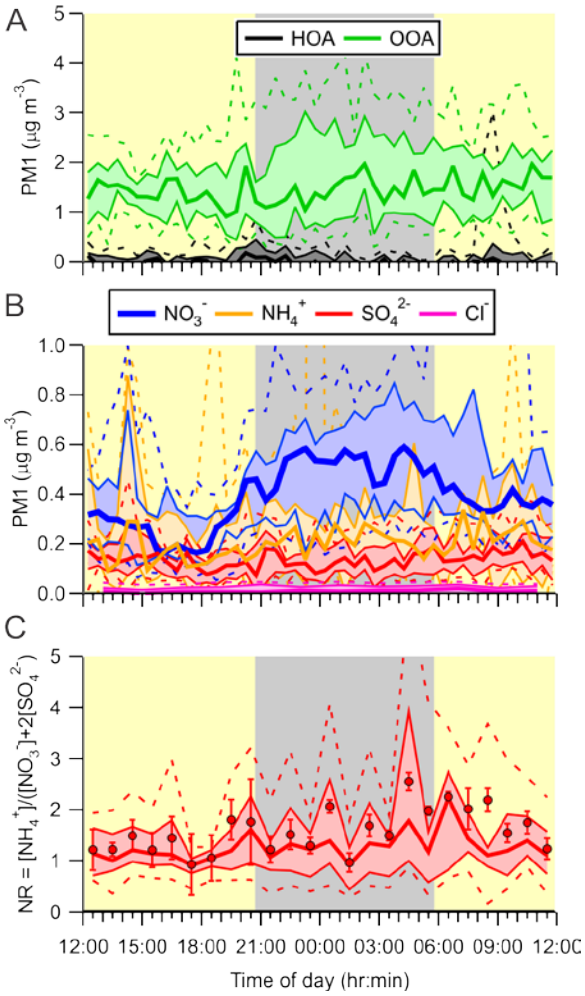

604

605 **Figure 6**. Diurnal averages of submicron (PM1) ACSM data. (**A**). Organic aerosol displayed
606 as hydrocarbon-like organic aerosol (HOA) and oxygenated organic aerosol (OOA) factors.
607 (**B**) Inorganic aerosol fractions. (C) Neutralization ratio (NR).

3.1.6 Hydrocarbon measurements

Mixing ratios of hydrocarbons were quantified during daytime and during the nights of August 2-3 and 3-4. A portion of the hydrocarbon data is shown in Figure 7A. Mixing ratios were generally smaller during the day than during night, due to the larger daytime mixing heights. On the nights of August 2/3 and 3/4, N_2O_5 was not detected, consistent with low $P(NO_3)$ values as O_3 mixing ratios approached zero (Figure 3). At the same time, there were strong NO_3 sinks present: Mixing ratios of α-pinene and limonene (left-hand axis) increased throughout the night, as thermal emissions continued into the shallow NBL. In contrast, mixing ratios of isoprene, whose emissions are driven by photosynthesis (Hewitt et al., 2011; Guenther et al., 1995), increased at the beginning of the nights and then decreased as isoprene was removed by oxidation with O_3 and NO_3 and by transport. Throughout both nights, the site was also influenced by anthropogenic hydrocarbons (e.g., isooctane and toluene, right-hand axis). Because synoptic conditions as judged from local wind speed and direction (Figure 3D) were similar on most of the other nights when hydrocarbons were not quantified, the data shown in Figure 7A were likely representative for much of the campaign.

The VOC data were not sufficiently comprehensive to allow an accurate determination of the NO_3 loss frequency to hydrocarbons, given by $\Sigma k_{NO3+VOC,i}[VOC]_i$. Shown in Figure 7B is the loss frequency of NO_3 to isoprene, calculated by multiplying its concentration with the NO_3 rate coefficient taken from Seinfeld and Pandis (2006). Loss of NO_3 to isoprene was a small sink compared to its loss to NO via R3 and NO_3 photolysis (R4) but was approximately on par with its indirect loss, i.e., the heterogeneous uptake of N_2O_5.

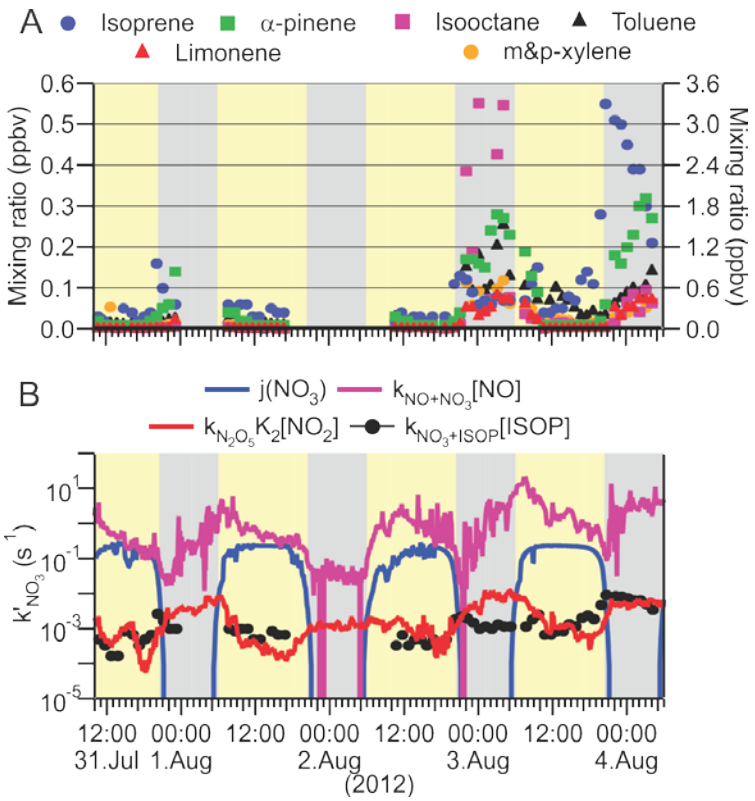

Figure 7. (A) Time series of selected VOC mixing ratios observed on the nights of August 2/3 and August 3/4, 2012. Biogenic VOCs (isoprene, α-pinene and limonene) are shown on the left-hand axis, and anthropogenic VOCs (isooctane, toluene and m&p-xylene) on the right-hand axis. The α-pinene and limonene measurements are semiquantitative. (B) Time series of NO_3 loss rate coefficients. ISOP = isoprene.

3.2 Analysis

3.2.1 Box model simulations of the nocturnal O_3 and O_x loss in the NBL

In initial simulations, the O_3 and NO_2 deposition rates were tuned until the median nocturnal O_x loss was reproduced. An O_3 dry deposition rate of 4×10^{-5} s^{-1} produced a simulation that reasonably matched the observations (Figure S-2). The magnitude of this rate corresponds to a NBL height of 50 m, the same mixing height that was frequently observed in balloon vertical profiles reported by Pisano et al. (1997). Modeling studies have assumed N_2O_5 and NO_3 deposition velocities of up to 2 cm s^{-1} in urban areas (Sander and Crutzen, 1996); adopting this value allows the dry deposition rate constants of N_2O_5 and NO_3 to be estimated at ~4×10^{-4} s^{-1}, which is on par with the estimated heterogeneous uptake rate constant of N_2O_5 on submicron aerosol.

Next, the generic biogenic VOC was added. For this, a biogenic hydrocarbon abundance of 1 ppbv at sunset (mostly isoprene – see Figure 7) and a (monoterpene) emission rate of 3×10^{5} molecules cm^{-3} s^{-1} based on the crop emission factor given by Guenther et al. (2012) into a 50 m deep NBL were assumed. This assumed flux gives a similar emission rate as the 0.3 ppbv increase over a 6 hour period observed on Aug 3-4 (Figure 7). The addition of this biogenic VOC only had a marginal effect on O_x (Figure S-3).

The simulations presented in Figures S-2 underpredict the observed loss of O_3, necessitating the addition of an NO source that results in selective removal of O_3 while preserving O_x. Since automobiles are the largest NO_x source in the region, a constant emission source of 95% NO and 5% NO_2 (Wild et al., 2017) was added and its magnitude varied. The NO_x source strength necessary to reproduce the median O_3 loss was ~1.1 ppbv hr^{-1}. The simulation results using these parameters are superimposed (in red) in Figure 4C. There is reasonable agreement between the simulations and observations of O_x and O_3 until ~3:00 (and between simulation and observation of NO, Figure S-4). This shows that the nocturnal O_3 and O_x loss can be rationalized without active NO_3 and N_2O_5 chemistry and suggests that NO_3, N_2O_5, and $ClNO_2$ did not contribute significantly to O_x and O_3 loss in the NBL.

3.2.2 Metrics of nocturnal nitrogen oxide chemistry: $P(NO_3)$, $\phi'(ClNO_2)$ and $\tau(N_2O_5)$

Nocturnal N_2O_5 chemistry was analyzed using several common metrics: the rate of NO_3 production by R1, $P(NO_3)=k_1[NO_2][O_3]$, the yield of $ClNO_2$ relative to the total amount of NO_3 formed at night, $\phi'(ClNO_2)$, and the steady state lifetime of N_2O_5, $\tau(N_2O_5)$.

The time of day dependence of $P(NO_3)$ is shown in Figure 8A. The NO_3 production rates were small (median values < 0.3 ppbv hr^{-1}) and were larger during the day than at night due to the low O_3 mixing ratios. After midnight, for example, the median $P(NO_3)$ was (55±23) pptv hr^{-1}. These are very modest NO_3 production rates for a site influenced by urban emissions. In a recent study on a mountain top in Hong Kong, for instance, $P(NO_3)$ in excess of 1 ppbv hr^{-1} was observed in polluted air (Brown et al., 2016).

The median integrated nocturnal NO_3 production over the course of the night was 940 pptv (Figure 8A, right hand axis), of which 600 pptv were produced before midnight. The amount of $ClNO_2$ produced relative to this amount, $\phi'(ClNO_2)$, was very small (median 0.17%, maximum 5.4% on the morning of August 2) and considerably less than reported by our group for Calgary (median 1.0%) (Mielke et al., 2016) and Pasadena, CA (median 12%) (Mielke et al., 2013).

A frequently calculated metric of nighttime nitrogen oxide chemistry is the steady state lifetimes of NO_3 and N_2O_5, $\tau(NO_3)$ and $\tau(N_2O_5)$ (Aldener et al., 2006; Heintz et al., 1996). The latter is calculated from (Brown et al., 2003; Brown and Stutz, 2012):

$$\tau(N_2O_5) = \frac{[N_2O_5]}{P(NO_3)} = \frac{[N_2O_5]}{k_1[NO_2][O_3]} \approx \left(k_{N_2O_5} + \frac{k_{NO_3}}{K_2[NO_2]} \right)^{-1} \quad (2)$$

Here, $k_{N_2O_5}$ and k_{NO_3} are the pseudo-first order loss-rate coefficients of N_2O_5 and NO_3 respectively, and K_2 is the equilibrium constant for equilibrium (R2).

A central assumption in this derivation is that NO_3, NO_2, and N_2O_5 more rapidly equilibrate than NO_3 is formed and either NO_3 or N_2O_5 are destroyed, i.e., NO_3+N_2O_5 are assumed to be in steady state with respect to production and loss. Brown et al. (2003) outlined potential pitfalls concerning the validity of the steady state approximation and recommended that box model simulations are carried out to evaluate if a steady state in N_2O_5 can be assumed. Using the median nocturnal NO_2 and O_3 mixing ratios of 7.5 ppbv and 18 to 5.0 ppbv, respectively,

a temperature of 286 K, and assumed N_2O_5 and NO_3 pseudo-first order loss frequencies of 1×10^{-3} s^{-1} and between 1×10^{-2} s^{-1} and 0 s^{-1}, the time to achieve steady state in N_2O_5 is 70 min or less (see S.I.). Thus, the steady state assumption is reasonable for this data set.

A key parameter in equation ((2) is the strongly temperature dependent equilibrium constant K_2 (Osthoff et al., 2007). At night, the air temperatures during this study were quite warm (median nocturnal minimum of +13 °C) and did not vary a lot between nights (Figure 8B). The warm temperatures shift equilibrium R2 away from N_2O_5 and towards NO_3 and NO_2, making losses via NO_3 (R3-R4 and R7) more competitive with the losses of N_2O_5 (that produce $ClNO_2$; R), i.e., the $\frac{k_{NO_3}}{K_2[NO_2]}$ term in equation 11 becomes large relative to $k_{N_2O_5}$. On the other hand, the relatively high NO_2 mixing ratios (median value 7.5±0.8 ppbv) shift the equilibrium towards N_2O_5. Thus, in spite of the relatively warm temperatures, the N_2O_5:NO_3 equilibrium ratios were large on aggregate (>15; Figure 8B), enabling $ClNO_2$ formation via R5.

The steady state lifetime of N_2O_5, $\tau(N_2O_5)$, is shown as a diurnal average in Figure 8C. The median $\tau(N_2O_5)$ at night was short (~1 min), and the 90th percentile peaked at a modest 7.6 min at sunrise, considerably shorter than observed above the NBL (Brown et al., 2006b) and at other ground sites (Wood et al., 2005; Crowley et al., 2010; Brown et al., 2016)

Superimposed on the right-hand side of Figure 8C are upper limits to the steady state lifetime of N_2O_5, calculated using the sum of pseudo first-order rate coefficients for the titration of NO_3 by NO ($k_3[NO]$, R3), NO_3 photolysis ($j(NO_3)$, R4), and NO_3 dry deposition ($k_{dep}(NO_3)$), all divided by the N_2O_5 over NO_3 ratio at equilibrium given by K_2NO_2 (Figure 8B), plus the pseudo first-order rate coefficient for N_2O_5 heterogeneous uptake ($k_{het}(N_2O_5)$, equation (1)) plus N_2O_5 dry deposition ($k_{dep}(N_2O_5)$).

$$\tau(N_2O_5) = \left(\frac{k_{NO_3}}{K_2[NO_2]} + k_{N_2O_5}\right)^{-1} < \left(\frac{k_3[NO] + j(NO_3) + k_{dep}(NO_3)}{K_2[NO_2]} + k_{het}(N_2O_5) + k_{dep}(N_2O_5)\right)^{-1} \quad (3)$$

The dry deposition rate constants were set to 4×10^{-4} s^{-1} (see section 3.2.1), which likely overestimates dry deposition during the day due to higher mixing heights; however, the error this introduces is negligible compared to the large daytime sinks such as NO_3 photolysis and its reaction with NO. Missing from equation (3) are losses of NO_3 to hydrocarbons (which was omitted because of the poor VOC data coverage) and terms for NO_3 and N_2O_5 wet (i.e., on cloud and rain droplets) deposition. Periods affected by precipitation or fog (shown in Figure 3D) were hence excluded from the calculation.

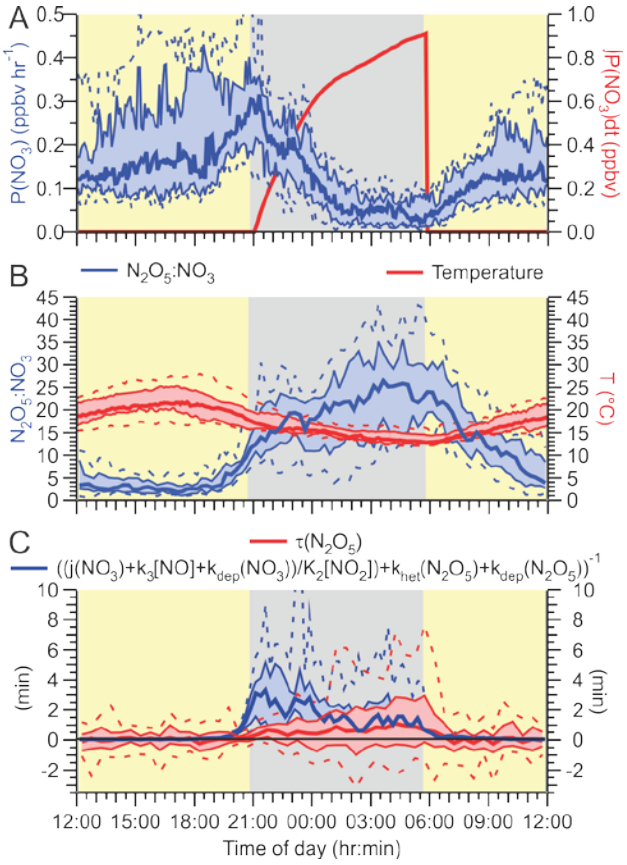

Figure 8. (**A**) NO_3 production rate $P(NO_3) = k_1[NO_2][O_3]$ as a function of time of day. The red line is the total amount NO_3 generated since sunset, $\int P(NO_3)dt$. (**B**) Equilibrium ratio of N_2O_5 to NO_3 calculated by multiplying the temperature-dependent equilibrium constant, K_2, with the NO_2 concentration, $[NO_2]$ (left axis), and air temperature (right axis). (**C**) Steady state lifetime of N_2O_5 (left axis) and upper limits calculated using equation (3) (right axis) as functions of time of day.

The median "observed" $\tau(N_2O_5)$ is below or equal to the upper limit calculation with equation (3) during both night and day. The largest discrepancy is observed at the beginning of the night, when oxidation of (unsaturated) hydrocarbons by NO_3 (R7) was likely most significant due to the presence of isoprene. It is also the time when the steady state approximation is most likely invalid.

3.2.3 Heterogeneous conversion of N_2O_5 to $ClNO_2$ on the night of August 1/2

Phillips et al. (2016) recently applied several methods to estimate the N_2O_5 uptake parameter (γ) and yield of $ClNO_2$ (ϕ) from ambient measurements of NO_3, N_2O_5, $ClNO_2$, and aerosol nitrate. One of these methods uses the covariance of $ClNO_2$ and aerosol nitrate production rates, $P(NO_3^-)$ and $P(ClNO_2)$:

$$\phi = 2(P(NO_3^-)/P(ClNO_2) +1)^{-1} \quad (4)$$

$$\gamma = 2(P(NO_3^-)+P(ClNO_2))/(c\ S_A\ [N_2O_5]) \quad (5)$$

In the above equation, c is the mean molecular speed of N_2O_5 ($\approx$ 237 m s^{-1}). The use of equations (4-5) assumes that the relevant properties of the air mass are conserved (i.e., identical upwind of and at the measurement location and affected identically by air masses mixing), that losses of measured species are not significant, that the efficiency of N_2O_5 uptake and production of $ClNO_2$ and NO_3^- is independent of particle size, and the absence of partitioning of $HNO_{3(g)}$ and aerosol nitrate between the gas and particle phases (Phillips et al., 2016). It is assumed further that production of nitrate from N_2O_5 uptake on refractory aerosol (that the ACSM does not quantify) is minimal.

In this data set, $ClNO_2$ and PM_1 nitrate rarely covaried (Figure 9); the only instance showing a modest correlation (r=0.66) is the time period prior to sunrise of August 2 (shown as red dots in Figure 9).

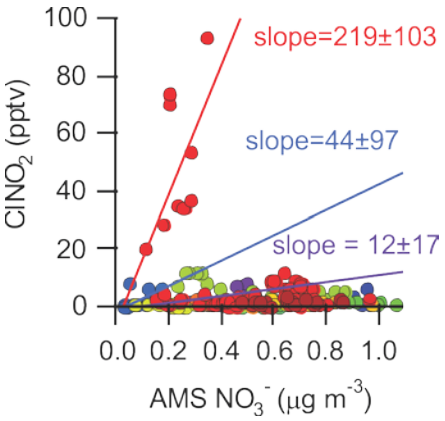

Figure 9. Scatter plot of $ClNO_2$ mixing ratios with submicron (PM_1) ACSM NO_3^- data. The slopes were calculated for three periods: Aug 2, 01:25 – 04:55 (red dots; slope = 219±103; ϕ = 0.72), July 23, 03:00 – 04:25 (blue dots slope = 44±97; ϕ = 0.21), and July 21, 02:25 – 05:20 (purple dots slope = 12±17; ϕ = 0.06).

The night of August 1-2 exhibited the highest nocturnal nitrogen oxide concentrations for the entire campaign. Winds were initially from the NW and relatively light (4.8±0.7 km hr^{-1}) and after 01:00 picked up in speed (to 8±1 km hr^{-1}) and shifted to the W. Judging from the HYbrid Single-Particle Lagrangian Integrated Trajectory (HYSPLIT) back trajectories (Draxler and Rolph, 2013), the upwind air had moved in from the coast, roughly from the direction of the city of Victoria, BC (Odame-Ankrah, 2015).

After sunset at ~21:00 local time, N_2O_5 levels started increasing and continued to increase until about 01:30 (Figure 3A). The steady state N_2O_5 lifetime at this time was the highest of the campaign, ~10 min. At 01:20, $ClNO_2$ mixing ratio increased from 20.4 pptv at 01:25 to 93.7 pptv at 04:55 and the aerosol nitrate content from 0.10 to 0.34 μg m^{-3} (40 to 127 pptv). During this time, N_2O_5 mixing ratios and PM_1 surface area density were relatively constant, 11±6 pptv and 67±4 μg m^{-3} (average ± standard deviation), respectively. The combined amount of N_2O_5, $ClNO_2$ and NO_3^- produced (172 pptv) is less than the amount of NO_3 produced from R1 which was 519 pptv during this period.

From equations (4) and (5), a $ClNO_2$ yield of ϕ = 0.7±0.3 and an N_2O_5 uptake probability of γ = 0.15±0.07 were calculated for this period. Both of these values are upper limits because

production of $ClNO_2$ from uptake of N_2O_5 on unquantified supermicron (i.e., > 0.5 μm) or refractory aerosol (which takes place simultaneously) is not accounted for.

A γ value of > 0.05 is greater than can be rationalized from laboratory and field studies (Chang et al., 2011) and is hence unrealistic. This suggests that $ClNO_2$ production took place predominantly on supermicron or refractory aerosol, which likely was comprised of mainly sea salt derived aerosol (Anlauf et al., 2006). On the other hand, if one assumes that all of the $ClNO_2$ is produced on supermicron or refractory aerosol such that $P(ClNO_2)$ on submicron aerosol equals 0 pptv s^{-1} (which is not unreasonable considering the absence of measurable amounts of aerosol chloride in this size fraction, see section 3.1.5), a γ value of 0.08±0.04 is calculated. This large value suggests very efficient N_2O_5 uptake (and conversion to aerosol nitrate) on the non-refractory submicron aerosol that night.

3.3 Impacts of $ClNO_2$ on radical production

Photolysis of $ClNO_2$ increases the rates of photochemical O_3 production (and hence worsen air quality) by producing NO_2 and reactive Cl atoms (reaction 6). The amounts of $ClNO_2$ available for photolysis in the morning (median 3.5 pptv at sunrise and 6.8 pptv at 08:00 local time) were too small to have had a measurable impact on local NO_2 concentrations (Figure 3C) but were sufficiently large to, at least occasionally, impact radical budgets.

Figure 10 shows the instantaneous radical production rates of Cl and OH, $P(Cl)=j(ClNO_2)\times[ClNO_2]$ and P(OH) from reaction of $O(^1D)+H_2O$. The latter was calculated from an assumed steady state in $O(^1D)$ with respect to its production from O_3 photolysis and reactions with N_2, O_2, and H_2O as described by Mielke et al. (2016). This analysis does not account for OH radical production from photolysis of nitrous acid or aldehydes and, hence, overestimates the importance of Cl radicals.

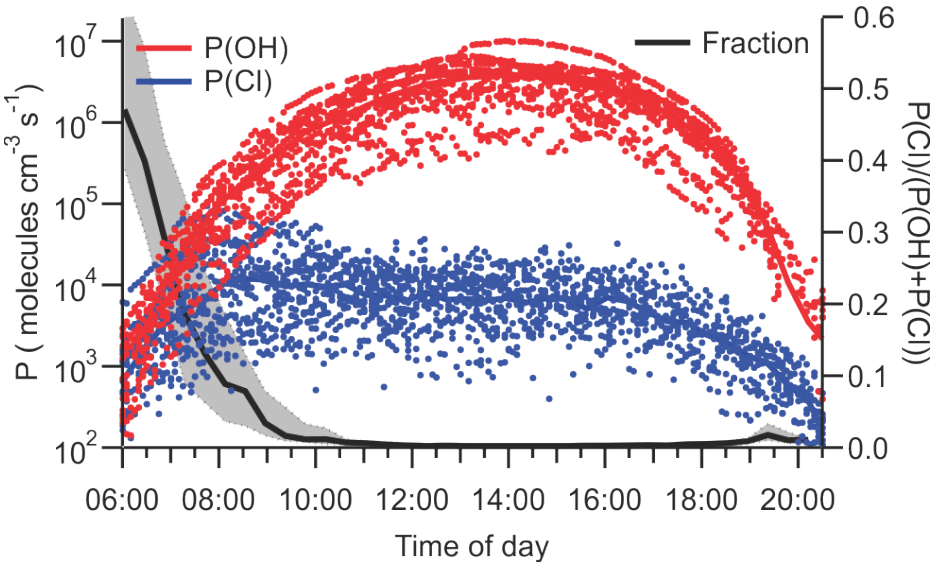

Figure 10. Plots of instantaneous rates of Cl (blue) and OH (red) radical production from $ClNO_2$ photolysis and reaction of O^1D, generated from O_3 photolysis, with H_2O and as a function of time of day. The fraction of radicals produced from $ClNO_2$ photolysis is shown in black. The solid line indicates median values, and shaded areas the 75th and 25th percentiles.

The largest P(Cl) values were observed on July 26, 07:45 local time (9.5×10^4 atoms cm^{-3} s^{-1}), accounting for 40% of the total radical production. The largest fraction of radicals produced from $ClNO_2$ photolysis was observed on the same day at 6:35 local time (74%, 7.8×10^3 atoms cm^{-3} s^{-1}). The photolysis of $ClNO_2$ produces a median value of 6.5×10^3 atoms cm^{-3} s^{-1} during daytime, which is negligibly small compared to the median P(OH) of 3.8×10^6 molecules cm^{-3} s^{-1} at noon.

4 Discussion

It is now well-established that $ClNO_2$ is an abundant nitrogen oxide in many regions of the troposphere (Table 3). The results presented in this paper are atypical in that they show consistently small $ClNO_2$ mixing ratios in spite of close proximity to sources, i.e., in a region where nearby oceanic emissions of sea salt aerosol and NO_x emissions from a megacity combine. In the following, factors contributing to the low $ClNO_2$ mixing ratios observed in this study and broader implications of $ClNO_2$ in the LFV are discussed.

The main reason for the low $ClNO_2$ mixing ratios observed in this work are the low nocturnal mixing ratios of O_3 and small NO_3 production rate, $P(NO_3)$, resulting from the stratification of the boundary layer at night and decoupling of the shallow NBL from the NRL. In the following, it is assumed that a boundary layer structure similar to those observed during PACIFIC 93 (Pisano et al., 1997; McKendry et al., 1997; Hayden et al., 1997) also existed on most measurement nights of this study. Once the nocturnal boundary layer formed at sunset, O_3 and O_x in the NBL were rapidly (lifetime of ~ 4 hours) removed. The box model simulations presented in section 3.2.1 show that this removal can be rationalized by dry deposition and titration of O_3 with NO and biogenic VOCs alone, leaving little room for nitrogen oxide chemistry to destroy O_3 or NO_2, for example, via heterogeneous formation of HONO which destroys NO_2 (Bröske et al., 2003; Stutz et al., 2004a; Indarto, 2012) or formation of N_2O_5 and subsequent heterogeneous hydrolysis which consumes 2 molecules of NO_2 and 1 molecule of O_3 (Brown et al., 2006a). It is the often complete absence of O_3 at night which distinguishes this data set from the other measurement locations for which $ClNO_2$ data have been reported, including continental sites where aerosol chloride is likely less abundant (Table 3).

A compounding factor in this study was the occasional formation of fog and occasional precipitation events. Fog droplets act as a very rapid sink for NO_3 and N_2O_5 (Osthoff et al., 2006), which shuts down $ClNO_2$ production, and may have also directly contributed episodically to $ClNO_2$ losses, for example on the morning of July 27. Overall, though, the contribution of fog to $ClNO_2$ losses in this data set was minor, as only 5% of the measurement period was impacted by fog. However, this potential $ClNO_2$ loss mechanism should be investigated further in future lab studies.

The rapid drop of $ClNO_2$ mixing ratio at around 06:00 of Aug 2 is interesting in that it coincided with a very brief precipitation event. Though an air mass shift cannot be ruled out,

this coincidence suggests the possibility that scavenging of $ClNO_2$ by rain droplets followed by hydrolysis may be a possible loss pathway. Scavenging of NO_3, N_2O_5, and $ClNO_2$ by rain droplets is currently not constrained by laboratory investigations (unlike other gases, such as SO_2 or NH_3 (Hannemann et al., 1995)). Similarly to fog, precipitation was not a major factor in this data set as it affected only 10% but may be in other locations or seasons that experience higher rainfall amounts.

An important observation is the lack of non-refractory PM_1 chloride (Figure 5B). This suggests that there was limited redistribution of chloride from acidification of sea salt aerosol onto other aerosol surfaces in this data set. Such a redistribution was observed, for example, during the Calnex-LA campaign, where the AMS measured a median chloride concentration of ~0.1 μg m^{-3} on non-refractory aerosol (Mielke et al., 2013). This in turn implies that the submicron aerosol surface did not significantly participate in the production of $ClNO_2$ from N_2O_5 uptake in the NBL, broadly consistent with the conclusions in section 3.2.3 and consistent with measurements of water-soluble aerosol components in the LFV during Pacific 2001 (Anlauf et al., 2006) that showed no evidence for chloride redistribution to PM_1 from larger particles where aerosol chloride was present.

The low observed $\tau(N_2O_5)$ levels are consistent with earlier studies that reported strong vertical gradients in $\tau(N_2O_5)$ due to elevated near-surface sinks from emissions by plants (i.e., monoterpenes) and automobiles (i.e., NO and butadiene (Curren et al., 2006)) that titrate NO_3 (Stutz et al., 2004b; Wang et al., 2006; Brown et al., 2007; Young et al., 2012). An emblematic example is the study by Wood et al. (2005) at a ground site east of the San Francisco Bay Area in January 2004: They observed relatively modest N_2O_5 mixing ratios of up to 200 pptv, corresponding to $\tau(N_2O_5) < 5$ min for the entire study period. Studies for which vertically resolved data were available (e.g., (Stutz et al., 2004b; Wang et al., 2006; Brown et al., 2007; Young et al., 2012; Tsai et al., 2014) generally showed higher N_2O_5 concentrations and hence larger $\tau(N_2O_5)$ aloft in the NRL than at the surface.

A different scenario likely played out aloft in the NRL, which would exhibit higher NO_3 production rates (via reactions 1) than the surface layer. Assuming levels of 20 ppbv of O_3 and NO_2 in the NRL (Pisano et al., 1997; McKendry et al., 1997), the NO_3 production rate would equal ~1.1 ppbv hr^{-1} in the NRL, roughly on par with values recently reported for Hong Kong, the current record holder for $ClNO_2$ mixing ratios (Brown et al., 2016; Wang et al.,

886 2016). Recent aircraft and tower studies have shown high rates of production of $ClNO_2$ aloft
887 (Riedel et al., 2013; Young et al., 2012), which likely also occurred in this work.

888 In contrast, the low mixing height of the NBL is conducive to high levels of biogenic
889 hydrocarbons (section 3.1.6). The nocturnal temperatures during this study were quite warm
890 and did not vary a lot between nights (Figure 8B). Emissions of monoterpenes, which are
891 reactive towards NO_3, are driven by a temperature-dependent process from storage tissue
892 within the plants at night (Guenther et al., 1995) and, hence, were likely substantial. Their
893 presence is likely responsible for the difference between the "observed" N_2O_5 steady
894 lifetimes, $\tau(N_2O_5)$, and upper limit calculated using equation (3) before midnight (Figure 8C).
895 Even if one assumes a relatively large uptake probability of γ=0.025 and accounts for the
896 large ratios of N_2O_5:NO_3, the loss rate of N_2O_5 on submicron aerosol was likely small in
897 comparison to losses via NO_3 for most of this data set (Figure 7B). Hence, only a small
898 fraction of the integrated nocturnal NO_3 production of 940 pptv resulted in $ClNO_2$ formation
899 at the surface.

900 Because of the relatively long lifetime of $ClNO_2$, the breakdown of the surface layer and
901 merging of the surface air with the NRL constituted itself as a $ClNO_2$ "morning peak" in a
902 similar manner as what has recently been reported at other locations (Tham et al., 2016;
903 Bannan et al., 2015; Faxon et al., 2015). This morning peak is rationalized by higher net
904 $ClNO_2$ production in the NRL; the break-up of this layer ~2 hours after sunrise then mixes
905 $ClNO_2$ down to the surface. Such a vertical mixing process was not seen during Calnex-LA
906 (Young et al., 2012; Tsai et al., 2014) where the NBL was sufficiently deep to prevent
907 complete O_3 removal and the $ClNO_2$ produced mixed down to the surface at night.

908 Assuming a 100 m deep NRL where $ClNO_2$ production takes place, a mixed layer height of
909 500 m by 08:00 (Pisano et al., 1997) and negligible destruction of $ClNO_2$ by photolysis
910 (which is reasonable as the lifetime of $ClNO_2$ with respect to photolysis is >4.6 hours at that
911 time of day), a morning increase in $ClNO_2$ mixing ratio by 40 pptv at the surface as seen on
912 the morning of July 26 suggests a pool of $ClNO_2$ in the NRL at sunrise of ~200 pptv, likely a
913 modest value considering that the (assumed) NO_3 production rate may have integrated to ~9
914 ppbv over the course of the night.

915 The largest nocturnal $ClNO_2$ mixing ratios were observed on July 22/23 and August 1/2. Both
916 of these nights exhibited high wind speeds and are counterexamples to what was observed on
917 other nights. We speculate that the higher levels of wind shear and turbulence altered the

nocturnal boundary layer structure which exhibited a greater degree of vertical mixing and higher O_3 concentrations at the surface. Consistent with this interpretation and the notion that an isolated NRL with higher net $ClNO_2$ production was absent on those nights, the mornings of July 23 and Aug 2 did not show a "morning peak". In contrast, low surface wind speeds were observed on the other nights, facilitating a stable and shallow nocturnal surface layer.

It is conceivable that a land-sea breeze effect transported air from a region closer to the coast that saw higher $ClNO_2$ production than at Abbotsford, i.e., that the $ClNO_2$ morning peaks are generated by horizontal as opposed to vertical transport. Large NO_3 mixing ratios have been reported at Saturna Island (McLaren et al., 2010), which strongly suggest that sizeable reservoirs of $ClNO_2$ form offshore at night. However, it is known how far inland these reservoirs extend. Considering the average wind speed in the morning (6 km hr^{-1}), distance to the coast (35 km), and close proximity (200 m) of the site to the bottom of the polluted NRL with documented high nocturnal pollution levels and early morning down mixing events, the vertical transport explanation is much more likely correct. Nevertheless, measurements of $ClNO_2$ at a site closer to the coast (e.g., at White Rock) would be beneficial.

Formation of $ClNO_2$ affects air quality through its photolysis which generates O_x, NO_x, and reactive Cl radicals in the morning, leading to higher net photochemical O_3 production (Sarwar et al., 2014). In spite of the low levels of $ClNO_2$ observed in this work, the production of radicals from its photodissociation was not always negligible (Figure 10). Conditions leading to O_3 exceedances did not develop during this study. If such conditions had developed, it is highly likely that this radical generation would have played a much greater role.

The data presented here suggest that higher rates of $ClNO_2$ and subsequent radical generation take place routinely in layers aloft, processes that are not directly observable at the surface but whose implications are felt as the ultimate product, O_3, is sufficiently long-lived to mix down to the surface (McKendry et al., 1997). Future studies should therefore target the NRL, for example through missed-approaches by aircraft, a blimp, or from a tall tower, especially during episodes of a developing O_3 exceedance event and also include composition measurements of refractory aerosol.

5 Summary and conclusions

In this paper, we have presented the first measurements of $ClNO_2$ and N_2O_5 mixing ratios in the LFV. In spite of the close proximity to NO_x (megacity of Vancouver) and sea salt aerosol (the Pacific Ocean) sources, $ClNO_2$ and N_2O_5 mixing ratios were small (maximum of 97 and 27 pptv, respectively) and smaller than observed at other measurement locations for which $ClNO_2$ abundances were reported. The low mixing ratios are explained through the removal of O_3 by deposition and titration with NO in a shallow nocturnal surface layer. Measurements of submicron aerosol composition by ACSM showed no enhancements of particle-phase chloride, which is in contrast to locations where high $ClNO_2$ mixing ratios were observed (such as Pasadena (Mielke et al., 2013)) and indicates that there was little processing and redistribution of sea salt derived chloride at this location. There is indirect evidence that higher production of $ClNO_2$ took place above the measurement site in the NRL, observed via downmixing after the break-up of the NBL in the morning, and highlights the need for future vertically resolved measurements (e.g., from an aircraft platform) of $ClNO_2$ and N_2O_5 mixing ratios in the LFV. Conditions leading to O_3 exceedences did not develop during the relatively short measurement period of 2 weeks, such that the full impact that nocturnal formation of $ClNO_2$ could have on radical production and NO_2 recycling remains unquantified.

Data availability

The data used in this study are available from the corresponding author upon request (hosthoff@ucalgary.ca).

Acknowledgments

This project was undertaken with the financial support of the Government of Canada through the Federal Department of the Environment. Ce projet a été réalisé avec l'appui financier du Gouvernement du Canada agissant par l'entremise du ministère fédéral de l'Environnement. Partial funding for this work was provided by the Natural Sciences and Engineering Research Council of Canada (NSERC) in the form of operating ("Discovery") and Research Tools and Instruments (RTI) grants. The Abbotsford field study was financially supported by a BC Clear research grant from the Fraser Basin Council of British Columbia and by Metro Vancouver.

References

Ainslie, B., and Steyn, D. G.: Spatiotemporal Trends in Episodic Ozone Pollution in the Lower Fraser Valley, British Columbia, in Relation to Mesoscale Atmospheric Circulation Patterns and Emissions, J. Appl. Met. Climatol., 46, 1631-1644, 10.1175/JAM2547.1, 2007.

Ainslie, B., Steyn, D. G., Reuten, C., and Jackson, P. L.: A Retrospective Analysis of Ozone Formation in the Lower Fraser Valley, British Columbia, Canada. Part II: Influence of Emissions Reductions on Ozone Formation, Atmosphere-Ocean, 51, 170-186, 10.1080/07055900.2013.782264, 2013.

Aldener, M., Brown, S. S., Stark, H., Williams, E. J., Lerner, B. M., Kuster, W. C., Goldan, P. D., Quinn, P. K., Bates, T. S., Fehsenfeld, F. C., and Ravishankara, A. R.: Reactivity and loss mechanisms of NO_3 and N_2O_5 in a polluted marine environment: Results from in situ measurements during New England Air Quality Study 2002, J. Geophys. Res., 111, D23S73, doi:10.1029/2006JD007252, 2006.

Alfarra, M. R., Coe, H., Allan, J. D., Bower, K. N., Boudries, H., Canagaratna, M. R., Jimenez, J. L., Jayne, J. T., Garforth, A. A., Li, S.-M., and Worsnop, D. R.: Characterization of urban and rural organic particulate in the Lower Fraser Valley using two Aerodyne Aerosol Mass Spectrometers, Atmos. Environm., 38, 5745-5758, 10.1016/j.atmosenv.2004.01.054, 2004.

Alicke, B., Geyer, A., Hofzumahaus, A., Holland, F., Konrad, S., Patz, H. W., Schafer, J., Stutz, J., Volz-Thomas, A., and Platt, U.: OH formation by HONO photolysis during the BERLIOZ experiment, J. Geophys. Res., 108, 8247, 10.1029/2001JD000579, 2003.

Anlauf, K., Li, S.-M., Leaitch, R., Brook, J., Hayden, K., Toom-Sauntry, D., and Wiebe, A.: Ionic composition and size characteristics of particles in the Lower Fraser Valley: Pacific 2001 field study, Atmos. Environm., 40, 2662-2675, 10.1016/j.atmosenv.2005.12.027, 2006.

1004 Bannan, T. J., Booth, A. M., Bacak, A., Muller, J. B. A., Leather, K. E., Le Breton, M., Jones,
1005 B., Young, D., Coe, H., Allan, J., Visser, S., Slowik, J. G., Furger, M., Prévôt, A. S. H., Lee,
1006 J., Dunmore, R. E., Hopkins, J. R., Hamilton, J. F., Lewis, A. C., Whalley, L. K., Sharp, T.,
1007 Stone, D., Heard, D. E., Fleming, Z. L., Leigh, R., Shallcross, D. E., and Percival, C. J.: The
1008 first UK measurements of nitryl chloride using a chemical ionization mass spectrometer in
1009 central London in the summer of 2012, and an investigation of the role of Cl atom oxidation,
1010 J. Geophys. Res., 120, 5638-5657, 10.1002/2014jd022629, 2015.

1011 Bart, M., Williams, D. E., Ainslie, B., McKendry, I., Salmond, J., Grange, S. K., Alavi-
1012 Shoshtari, M., Steyn, D., and Henshaw, G. S.: High Density Ozone Monitoring Using Gas
1013 Sensitive Semi-Conductor Sensors in the Lower Fraser Valley, British Columbia, Environm.
1014 Sci. Technol., 48, 3970-3977, 10.1021/es404610t, 2014.

1015 Behnke, W., George, C., Scheer, V., and Zetzsch, C.: Production and decay of $ClNO_2$, from
1016 the reaction of gaseous N_2O_5 with NaCl solution: Bulk and aerosol experiments, J. Geophys.
1017 Res., 102, 3795-3804, 10.1029/96JD03057 1997.

1018 Bertram, T. H., and Thornton, J. A.: Toward a general parameterization of N_2O_5 reactivity on
1019 aqueous particles: the competing effects of particle liquid water, nitrate and chloride, Atmos.
1020 Chem. Phys., 9, 8351-8363, 10.5194/acp-9-8351-2009, 2009.

1021 Biesenthal, T. A., Wu, Q., Shepson, P. B., Wiebe, H. A., Anlauf, K. G., and Mackay, G. I.: A
1022 study of relationships between isoprene, its oxidation products, and ozone, in the Lower
1023 Fraser Valley, BC, Atmos. Environm., 31, 2049-2058, 10.1016/S1352-2310(96)00318-4,
1024 1997.

1025 Boudries, H., Canagaratna, M. R., Jayne, J. T., Alfarra, M. R., Allan, J., Bower, K. N., Coe,
1026 H., Pryor, S. C., Jimenez, J. L., Brook, J. R., Li, S., and Worsnop, D. R.: Chemical and
1027 physical processes controlling the distribution of aerosols in the Lower Fraser Valley, Canada,

during the Pacific 2001 field campaign, Atmos. Environm., 38, 5759-5774, 10.1016/j.atmosenv.2004.01.057, 2004.

Brook, J. R., Strawbridge, K. B., Snyder, B. J., Boudries, H., Worsnop, D., Sharma, S., Anlauf, K., Lu, G., and Hayden, K.: Towards an understanding of the fine particle variations in the LFV: integration of chemical, physical and meteorological observations, Atmos. Environm., 38, 5775-5788, 10.1016/j.atmosenv.2004.01.056, 2004.

Bröske, R., Kleffmann, J., and Wiesen, P.: Heterogeneous conversion of NO_2 on secondary organic aerosol surfaces: A possible source of nitrous acid (HONO) in the atmosphere?, Atmos. Chem. Phys., 3, 469-474, 10.5194/acp-3-469-2003, 2003.

Brown, S. S., Stark, H., Ciciora, S. J., and Ravishankara, A. R.: In-situ measurement of atmospheric NO_3 and N_2O_5 via cavity ring-down spectroscopy, Geophys. Res. Lett., 28, 3227-3230, 10.1029/2001GL013303, 2001.

Brown, S. S., Stark, H., Ciciora, S. J., McLaughlin, R. J., and Ravishankara, A. R.: Simultaneous in situ detection of atmospheric NO_3 and N_2O_5 via cavity ring-down spectroscopy, Rev. Sci. Instrum., 73, 3291-3301, 10.1063/1.1499214, 2002.

Brown, S. S., Stark, H., and Ravishankara, A. R.: Applicability of the steady state approximation to the interpretation of atmospheric observations of NO_3 and N_2O_5, J. Geophys. Res., 108, 4539, 10.1029/2003JD003407, 2003.

Brown, S. S., Neuman, J. A., Ryerson, T. B., Trainer, M., Dube, W. P., Holloway, J. S., Warneke, C., de Gouw, J. A., Donnelly, S. G., Atlas, E., Matthew, B., Middlebrook, A. M., Peltier, R., Weber, R. J., Stohl, A., Meagher, J. F., Fehsenfeld, F. C., and Ravishankara, A. R.: Nocturnal odd-oxygen budget and its implications for ozone loss in the lower troposphere, Geophys. Res. Lett., 33, L08801, 10.1029/2006GL025900, 2006a.

1051 Brown, S. S., Ryerson, T. B., Wollny, A. G., Brock, C. A., Peltier, R., Sullivan, A. P., Weber,
1052 R. J., Dube, W. P., Trainer, M., Meagher, J. F., Fehsenfeld, F. C., and Ravishankara, A. R.:
1053 Variability in nocturnal nitrogen oxide processing and its role in regional air quality, Science,
1054 311, 67-70, 10.1126/science.1120120 2006b.

1055 Brown, S. S., Dube, W. P., Osthoff, H. D., Stutz, J., Ryerson, T. B., Wollny, A. G., Brock, C.
1056 A., Warneke, C., De Gouw, J. A., Atlas, E., Neuman, J. A., Holloway, J. S., Lerner, B. M.,
1057 Williams, E. J., Kuster, W. C., Goldan, P. D., Angevine, W. M., Trainer, M., Fehsenfeld, F.
1058 C., and Ravishankara, A. R.: Vertical profiles in NO_3 and N_2O_5 measured from an aircraft:
1059 Results from the NOAA P-3 and surface platforms during the New England Air Quality Study
1060 2004, J. Geophys. Res., 112, D22304, 10.1029/2007JD008883, 2007.

1061 Brown, S. S., and Stutz, J.: Nighttime radical observations and chemistry, Chem. Soc. Rev.,
1062 41, 6405-6447, 10.1039/c2cs35181a, 2012.

1063 Brown, S. S., Thornton, J. A., Keene, W. C., Pszenny, A. A. P., Sive, B. C., Dubé, W. P.,
1064 Wagner, N. L., Young, C. J., Riedel, T. P., Roberts, J. M., VandenBoer, T. C., Bahreini, R.,
1065 Öztürk, F., Middlebrook, A. M., Kim, S., Hübler, G., and Wolfe, D. E.: Nitrogen, Aerosol
1066 Composition, and Halogens on a Tall Tower (NACHTT): Overview of a wintertime air
1067 chemistry field study in the front range urban corridor of Colorado, J. Geophys. Res., 118,
1068 8067-8085, 10.1002/jgrd.50537, 2013.

1069 Brown, S. S., Dubé, W. P., Tham, Y. J., Zha, Q., Xue, L., Poon, S., Wang, Z., Blake, D. R.,
1070 Tsui, W., Parrish, D. D., and Wang, T.: Nighttime chemistry at a high altitude site above
1071 Hong Kong, J. Geophys. Res.-Atmos., 121, 2457-2475, 10.1002/2015jd024566, 2016.

1072 Chang, W. L., Bhave, P. V., Brown, S. S., Riemer, N., Stutz, J., and Dabdub, D.:
1073 Heterogeneous Atmospheric Chemistry, Ambient Measurements, and Model Calculations of

N_2O_5: A Review, Aerosol Sci. Technol., 45, 655 - 685, 10.1080/02786826.2010.551672, 2011.

Crowley, J. N., Schuster, G., Pouvesle, N., Parchatka, U., Fischer, H., Bonn, B., Bingemer, H., and Lelieveld, J.: Nocturnal nitrogen oxides at a rural mountain-site in south-western Germany, Atmos. Chem. Phys., 10, 2795-2812, 10.5194/acp-10-2795-2010, 2010.

Curren, K. C., Dann, T. F., and Wang, D. K.: Ambient air 1,3-butadiene concentrations in Canada (1995–2003): seasonal, day of week variations, trends, and source influences, Atmos. Environm., 40, 170-181, 10.1016/j.atmosenv.2005.09.025, 2006.

Davidovits, P., Kolb, C. E., Williams, L. R., Jayne, J. T., and Worsnop, D. R.: Mass accommodation and chemical reactions at gas-liquid interfaces, Chem. Rev., 106, 1323-1354, 2006.

HYSPLIT (HYbrid Single-Particle Lagrangian Integrated Trajectory) Model access via NOAA ARL READY Website http://ready.arl.noaa.gov/HYSPLIT.php, 2013.

Drewitt, G. B., Curren, K., Steyn, D. G., Gillespie, T. J., and Niki, H.: Measurement of biogenic hydrocarbon emissions from vegetation in the Lower Fraser Valley, British Columbia, Atmos. Environm., 32, 3457-3466, 10.1016/S1352-2310(98)00043-0, 1998.

Dubé, W. P., Brown, S. S., Osthoff, H. D., Nunley, M. R., Ciciora, S. J., Paris, M. W., McLaughlin, R. J., and Ravishankara, A. R.: Aircraft instrument for simultaneous, in situ measurement of NO_3 and N_2O_5 via pulsed cavity ring-down spectroscopy, Rev. Sci. Instrum., 77, 034101, 10.1063/1.2176058, 2006.

Edwards, P. M., Brown, S. S., Roberts, J. M., Ahmadov, R., Banta, R. M., deGouw, J. A., Dube, W. P., Field, R. A., Flynn, J. H., Gilman, J. B., Graus, M., Helmig, D., Koss, A., Langford, A. O., Lefer, B. L., Lerner, B. M., Li, R., Li, S.-M., McKeen, S. A., Murphy, S. M.,

Parrish, D. D., Senff, C. J., Soltis, J., Stutz, J., Sweeney, C., Thompson, C. R., Trainer, M. K., Tsai, C., Veres, P. R., Washenfelder, R. A., Warneke, C., Wild, R. J., Young, C. J., Yuan, B., and Zamora, R.: High winter ozone pollution from carbonyl photolysis in an oil and gas basin, Nature, 514, 351-354, 10.1038/nature13767, 2014.

Faxon, C., Bean, J., and Ruiz, L.: Inland Concentrations of Cl_2 and $ClNO_2$ in Southeast Texas Suggest Chlorine Chemistry Significantly Contributes to Atmospheric Reactivity, Atmosphere, 6, 1487, 10.3390/atmos6101487, 2015.

Finlayson-Pitts, B. J., Ezell, M. J., and Pitts, J. N.: Formation Of Chemically Active Chlorine Compounds By Reactions Of Atmospheric NaCl Particles With Gaseous N_2O_5 And $ClONO_2$, Nature, 337, 241-244, 10.1038/337241a0 1989.

Geyer, A., and Stutz, J.: Vertical profiles of NO_3, N_2O_5, O_3, and NO_x in the nocturnal boundary layer: 2. Model studies on the altitude dependence of composition and chemistry, J. Geophys. Res., 109, D12307, doi:12310.11029/12003JD004211, 2004.

Ghosh, B., Papanastasiou, D. K., Talukdar, R. K., Roberts, J. M., and Burkholder, J. B.: Nitryl Chloride ($ClNO_2$): UV/Vis Absorption Spectrum between 210 and 296 K and O(^{3}P) Quantum Yield at 193 and 248 nm, J. Phys. Chem. A, 116, 5796-5805, 10.1021/jp207389y, 2012.

Guenther, A., Hewitt, C. N., Erickson, D., Fall, R., Geron, C., Graedel, T., Harley, P., Klinger, L., Lerdau, M., McKay, W. A., Pierce, T., Scholes, B., Steinbrecher, R., Tallamraju, R., Taylor, J., and Zimmerman, P.: A Global-Model Of Natural Volatile Organic-Compound Emissions, J. Geophys. Res., 100, 8873-8892, 10.1029/94JD02950, 1995.

Guenther, A. B., Jiang, X., Heald, C. L., Sakulyanontvittaya, T., Duhl, T., Emmons, L. K., and Wang, X.: The Model of Emissions of Gases and Aerosols from Nature version 2.1 (MEGAN2.1): an extended and updated framework for modeling biogenic emissions, Geosci. Model Dev., 5, 1471-1492, 10.5194/gmd-5-1471-2012, 2012.

1121 Gurren, K., Gillespie, T., Steyn, D., Dann, T., and Wang, D.: Biogenic isoprene in the Lower
1122 Fraser Valley, British Columbia, J. Geophys. Res.-Atmos., 103, 25467-25477,
1123 10.1029/98jd01214, 1998.

1124 Hannemann, A. U., Mitra, S. K., and Pruppacher, H. R.: On the scavenging of gaseous
1125 nitrogen compounds by large and small rain drops 1. A wind tunnel and theoretical study of
1126 the uptake and desorption of NH_3 in the presence of CO_2, J. Atmos. Chem., 21, 293-307,
1127 10.1007/bf00696760, 1995.

1128 Hayden, K. L., Anlauf, K. G., Hoff, R. M., Strapp, J. W., Bottenheim, J. W., Wiebe, H. A.,
1129 Froude, F. A., Martin, J. B., Steyn, D. G., and McKendry, I. G.: The vertical chemical and
1130 meteorological structure of the boundary layer in the Lower Fraser Valley during Pacific '93,
1131 Atmos. Environm., 31, 2089-2105, 10.1016/S1352-2310(96)00300-7, 1997.

1132 Hayden, K. L., Anlauf, K. G., Li, S. M., Macdonald, A. M., Bottenheim, J. W., Brook, J. R.,
1133 and Wiebe, H. A.: Characterization of gaseous nitrogen oxides in the Lower Fraser Valley
1134 during Pacific 2001, Atmos. Environm., 38, 5811-5823, 10.1016/j.atmosenv.2003.12.048,
1135 2004.

1136 Heintz, F., Platt, U., Flentje, H., and Dubois, R.: Long-term observation of nitrate radicals at
1137 the Tor station, Kap Arkona (Rugen), J. Geophys. Res., 101, 22891-22910,
1138 10.1029/96JD01549, 1996.

1139 Hewitt, C. N., Ashworth, K., Boynard, A., Guenther, A., Langford, B., MacKenzie, A. R.,
1140 Misztal, P. K., Nemitz, E., Owen, S. M., Possell, M., Pugh, T. A. M., Ryan, A. C., and Wild,
1141 O.: Ground-level ozone influenced by circadian control of isoprene emissions, Nat. Geosci.,
1142 4, 671-674, 10.1038/ngeo1271, 2011.

1143 Hofzumahaus, A., Kraus, A., and Muller, M.: Solar actinic flux spectroradiometry: a
1144 technique for measuring photolysis frequencies in the atmosphere, Appl. Optics, 38, 4443-
1145 4460, 10.1364/AO.38.004443, 1999.

1146 Indarto, A.: Heterogeneous reactions of HONO formation from NO_2 and HNO_3: a review,
1147 Res. Chem. Intermed., 38, 1029-1041, 10.1007/s11164-011-0439-z, 2012.

1148 Jimenez, J. L., Canagaratna, M. R., Donahue, N. M., Prevot, A. S. H., Zhang, Q., Kroll, J. H.,
1149 DeCarlo, P. F., Allan, J. D., Coe, H., Ng, N. L., Aiken, A. C., Docherty, K. S., Ulbrich, I. M.,
1150 Grieshop, A. P., Robinson, A. L., Duplissy, J., Smith, J. D., Wilson, K. R., Lanz, V. A.,
1151 Hueglin, C., Sun, Y. L., Tian, J., Laaksonen, A., Raatikainen, T., Rautiainen, J., Vaattovaara,
1152 P., Ehn, M., Kulmala, M., Tomlinson, J. M., Collins, D. R., Cubison, M. J., E., Dunlea, J.,
1153 Huffman, J. A., Onasch, T. B., Alfarra, M. R., Williams, P. I., Bower, K., Kondo, Y.,
1154 Schneider, J., Drewnick, F., Borrmann, S., Weimer, S., Demerjian, K., Salcedo, D., Cottrell,
1155 L., Griffin, R., Takami, A., Miyoshi, T., Hatakeyama, S., Shimono, A., Sun, J. Y., Zhang, Y.
1156 M., Dzepina, K., Kimmel, J. R., Sueper, D., Jayne, J. T., Herndon, S. C., Trimborn, A. M.,
1157 Williams, L. R., Wood, E. C., Middlebrook, A. M., Kolb, C. E., Baltensperger, U., and
1158 Worsnop, D. R.: Evolution of Organic Aerosols in the Atmosphere, Science, 326, 1525-1529,
1159 10.1126/science.1180353, 2009.

1160 Kercher, J. P., Riedel, T. P., and Thornton, J. A.: Chlorine activation by N_2O_5: simultaneous,
1161 in situ detection of $ClNO_2$ and N_2O_5 by chemical ionization mass spectrometry, Atmospheric
1162 Measurement Techniques, 2, 193-204, 10.5194/amt-2-193-2009, 2009.

1163 Kim, M. J., Farmer, D. K., and Bertram, T. H.: A controlling role for the air-sea interface in
1164 the chemical processing of reactive nitrogen in the coastal marine boundary layer, Proc. Natl.
1165 Acad. Sci. U.S.A., 111, 3943-3948, 10.1073/pnas.1318694111, 2014.

1166 Kleinman, L., Lee, Y.-N., Springston, S. R., Nunnermacker, L., Zhou, X., Brown, R.,
1167 Hallock, K., Klotz, P., Leahy, D., Lee, J. H., and Newman, L.: Ozone formation at a rural site
1168 in the southeastern United States, J. Geophys. Res.-Atmos., 99, 3469-3482,
1169 10.1029/93jd02991, 1994.

1170 Knipping, E. M., and Dabdub, D.: Impact of chlorine emissions from sea-salt aerosol on
1171 coastal urban ozone, Environm. Sci. Technol., 37, 275-284, 10.1021/es025793z 2003.

1172 Koehler, G., and Wassenaar, L. I.: The stable isotopic composition ($^{37}Cl/^{35}Cl$) of dissolved
1173 chloride in rainwater, Applied Geochemistry, 25, 91-96, 10.1016/j.apgeochem.2009.10.004,
1174 2010.

1175 Lin, C. H., Lai, C. H., Wu, Y. L., and Chen, M. J.: Simple model for estimating dry
1176 deposition velocity of ozone and its destruction in a polluted nocturnal boundary layer,
1177 Atmos. Environm., 44, 4364-4371, 10.1016/j.atmosenv.2010.07.053, 2010.

1178 Logan, J. A.: Ozone in rural areas of the United States, J. Geophys. Res.-Atmos., 94, 8511-
1179 8532, 10.1029/JD094iD06p08511, 1989.

1180 Madronich, S., and Flocke, S.: Theoretical Estimation of Biologically Effective UV Radiation
1181 at the Earth's Surface, in: Solar Ultraviolet Radiation, edited by: Zerefos, C., and Bais, A.,
1182 NATO ASI Series, Springer Berlin Heidelberg, 23-48, 1997.

1183 McKendry, I. G., Steyn, D. G., Lundgren, J., Hoff, R. M., Strapp, W., Anlauf, K., Froude, F.,
1184 Martin, J. B., Banta, R. M., and Olivier, L. D.: Elevated ozone layers and vertical down-
1185 mixing over the Lower Fraser Valley, BC, Atmos. Environm., 31, 2135-2146,
1186 10.1016/S1352-2310(96)00127-6, 1997.

McLaren, R., Salmon, R. A., Liggio, J., Hayden, K. L., Anlauf, K. G., and Leaitch, W. R.: Nighttime chemistry at a rural site in the Lower Fraser Valley, Atmos. Environm., 38, 5837-5848, 10.1016/j.atmosenv.2004.03.074, 2004.

McLaren, R., Wojtal, P., Majonis, D., McCourt, J., Halla, J. D., and Brook, J.: NO_3 radical measurements in a polluted marine environment: links to ozone formation, Atmos. Chem. Phys., 10, 4187-4206, 10.5194/acp-10-4187-2010, 2010.

Mielke, L. H., Furgeson, A., and Osthoff, H. D.: Observation of $ClNO_2$ in a mid-continental urban environment, Environm. Sci. Technol., 45, 8889-8896, 10.1021/es201955u, 2011.

Mielke, L. H., and Osthoff, H. D.: On quantitative measurements of peroxycarboxylic nitric anhydride mixing ratios by thermal dissociation chemical ionization mass spectrometry, Int. J. Mass Spectrom., 310, 1-9, 10.1016/j.ijms.2011.10.005, 2012.

Mielke, L. H., Stutz, J., Tsai, C., Hurlock, S. C., Roberts, J. M., Veres, P. R., Froyd, K. D., Hayes, P. L., Cubison, M. J., Jimenez, J. L., Washenfelder, R. A., Young, C. J., Gilman, J. B., de Gouw, J. A., Flynn, J. H., Grossberg, N., Lefer, B. L., Liu, J., Weber, R. J., and Osthoff, H. D.: Heterogeneous formation of nitryl chloride and its role as a nocturnal NO_x reservoir species during CalNex-LA 2010, J. Geophys. Res., 118, 10638-10652, 10.1002/jgrd.50783, 2013.

Mielke, L. H., Furgeson, A., Odame-Ankrah, C. A., and Osthoff, H. D.: Ubiquity of $ClNO_2$ in the nocturnal boundary layer of Calgary, AB, Canada, Canadian Journal of Chemistry, 94, 414-423, 10.1139/cjc-2015-0426, 2016.

Neu, U., Kunzle, T., and Wanner, H.: On the relation between ozone storage in the residual layer and daily variation in near-surface ozone concentration — A case study, Bound.-Layer Meteor., 69, 221-247, 10.1007/bf00708857, 1994.

Ng, N. L., Herndon, S. C., Trimborn, A., Canagaratna, M. R., Croteau, P. L., Onasch, T. B., Sueper, D., Worsnop, D. R., Zhang, Q., Sun, Y. L., and Jayne, J. T.: An Aerosol Chemical Speciation Monitor (ACSM) for Routine Monitoring of the Composition and Mass Concentrations of Ambient Aerosol, Aerosol Sci. Technol., 45, 780-794, 10.1080/02786826.2011.560211, 2011.

Odame-Ankrah, C. A., and Osthoff, H. D.: A compact diode laser cavity ring-down spectrometer for atmospheric measurements of NO_3 and N_2O_5 with automated zeroing and calibration, Appl. Spectrosc., 65, 1260-1268, 10.1366/11-06384, 2011.

Odame-Ankrah, C. A.: Improved detection instrument for nitrogen oxide species, Ph.D., Chemistry, University of Calgary, http://hdl.handle.net/11023/2006, Calgary, 2015.

Osthoff, H. D., Sommariva, R., Baynard, T., Pettersson, A., Williams, E. J., Lerner, B. M., Roberts, J. M., Stark, H., Goldan, P. D., Kuster, W. C., Bates, T. S., Coffman, D., Ravishankara, A. R., and Brown, S. S.: Observation of daytime N_2O_5 in the marine boundary layer during New England Air Quality Study - Intercontinental Transport and Chemical Transformation 2004, J. Geophys. Res., 111, D23S14, doi:10.1029/2006JD007593., 2006.

Osthoff, H. D., Pilling, M. J., Ravishankara, A. R., and Brown, S. S.: Temperature dependence of the NO_3 absorption cross-section above 298 K and determination of the equilibrium constant for NO_3+NO_2 <-> N_2O_5 at atmospherically relevant conditions, Phys. Chem. Chem. Phys., 9, 5785-5793, 10.1039/b709193a, 2007.

Osthoff, H. D., Roberts, J. M., Ravishankara, A. R., Williams, E. J., Lerner, B. M., Sommariva, R., Bates, T. S., Coffman, D., Quinn, P. K., Stark, H., Burkholder, J. B., Talukdar, R. K., Meagher, J., Fehsenfeld, F. C., and Brown, S. S.: High levels of nitryl chloride in the polluted subtropical marine boundary layer, Nat. Geosci., 1, 324-328, 10.1038/ngeo177, 2008.

1234 Paul, D., Furgeson, A., and Osthoff, H. D.: Measurement of total alkyl and peroxy nitrates by
1235 thermal decomposition cavity ring-down spectroscopy, Rev. Sci. Instrum., 80, 114101,
1236 10.1063/1.3258204 2009.

1237 Paul, D., and Osthoff, H. D.: Absolute Measurements of Total Peroxy Nitrate Mixing Ratios
1238 by Thermal Dissociation Blue Diode Laser Cavity Ring-Down Spectroscopy, Anal. Chem.,
1239 82, 6695-6703, 10.1021/ac101441z, 2010.

1240 Phillips, G. J., Tang, M. J., Thieser, J., Brickwedde, B., Schuster, G., Bohn, B., Lelieveld, J.,
1241 and Crowley, J. N.: Significant concentrations of nitryl chloride observed in rural continental
1242 Europe associated with the influence of sea salt chloride and anthropogenic emissions,
1243 Geophys. Res. Lett., 39, L10811, 10.1029/2012gl051912, 2012.

1244 Phillips, G. J., Thieser, J., Tang, M. J., Sobanski, N., Schuster, G., Fachinger, J., Drewnick,
1245 F., Borrmann, S., Bingemer, H., Lelieveld, J., and Crowley, J. N.: Estimating N_2O_5 uptake
1246 coefficients using ambient measurements of NO_3, N_2O_5, $ClNO_2$ and particle-phase nitrate,
1247 Atmos. Chem. Phys., 16, 13231-13249, 10.5194/acp-16-13231-2016, 2016.

1248 Pisano, J. T., McKendry, I., Steyn, D. G., and Hastie, D. R.: Vertical nitrogen dioxide and
1249 ozone concentrations measured from a tethered balloon in the Lower Fraser Valley, Atmos.
1250 Environm., 31, 2071-2078, 10.1016/S1352-2310(96)00146-X, 1997.

1251 Pryor, S. C., Barthelmie, R. J., Hoff, R. M., Sakiyama, S., Simpson, R., and Steyn, D.:
1252 REVEAL: Characterizing fine aerosols in the Fraser Valley, BC, Atmosphere-Ocean, 35,
1253 209-227, 10.1080/07055900.1997.9649592, 1997.

1254 Pryor, S. C., and Barthelmie, R. J.: REVEAL II: Seasonality and spatial variability of particle
1255 and visibility conditions in the Fraser Valley, Sci. Tot. Environm., 257, 95-110,
1256 10.1016/S0048-9697(00)00490-3, 2000.

1257 Pryor, S. C., Barthelmie, R. J., Schoof, J. T., Binkowski, F. S., Delle Monache, L., and Stull,
1258 R.: Modeling the impact of sea-spray on particle concentrations in a coastal city, Sci. Tot.
1259 Environm., 391, 132-142, 10.1016/j.scitotenv.2007.10.059, 2008.

1260 Raff, J. D., Njegic, B., Chang, W. L., Gordon, M. S., Dabdub, D., Gerber, R. B., and
1261 Finlayson-Pitts, B. J.: Chlorine activation indoors and outdoors via surface-mediated reactions
1262 of nitrogen oxides with hydrogen chloride, Proc. Natl. Acad. Sci. U.S.A., 106, 13647-13654,
1263 10.1073/pnas.0904195106, 2009.

1264 Riedel, T. P., Bertram, T. H., Crisp, T. A., Williams, E. J., Lerner, B. M., Vlasenko, A., Li,
1265 S.-M., Gilman, J. B., de Gouw, J., Bon, D. M., Wagner, N. L., Brown, S. S., and Thornton, J.
1266 A.: Nitryl Chloride and Molecular Chlorine in the Coastal Marine Boundary Layer,
1267 Environm. Sci. Technol., 46, 10463-10470, 10.1021/es204632r, 2012a.

1268 Riedel, T. P., Bertram, T. H., Ryder, O. S., Liu, S., Day, D. A., Russell, L. M., Gaston, C. J.,
1269 Prather, K. A., and Thornton, J. A.: Direct N_2O_5 reactivity measurements at a polluted coastal
1270 site, Atmos. Chem. Phys., 12, 2959-2968, 10.5194/acp-12-2959-2012, 2012b.

1271 Riedel, T. P., Wagner, N. L., Dubé, W. P., Middlebrook, A. M., Young, C. J., Öztürk, F.,
1272 Bahreini, R., VandenBoer, T. C., Wolfe, D. E., Williams, E. J., Roberts, J. M., Brown, S. S.,
1273 and Thornton, J. A.: Chlorine activation within urban or power plant plumes: Vertically
1274 resolved $ClNO_2$ and Cl_2 measurements from a tall tower in a polluted continental setting, J.
1275 Geophys. Res., 118, 8702-8715, 10.1002/jgrd.50637, 2013.

1276 Roberts, J. M., Osthoff, H. D., Brown, S. S., Ravishankara, A. R., Coffman, D., Quinn, P. K.,
1277 and Bates, T. S.: Laboratory Studies of Products of N_2O_5 Uptake on Cl^- Containing
1278 Substrates, Geophys. Res. Lett., 36, L20808, 10.1029/2009GL040448, 2009.

1279 Ryder, O. S., Ault, A. P., Cahill, J. F., Guasco, T. L., Riedel, T. P., Cuadra-Rodriguez, L. A.,
1280 Gaston, C. J., Fitzgerald, E., Lee, C., Prather, K. A., and Bertram, T. H.: On the Role of

Particle Inorganic Mixing State in the Reactive Uptake of N_2O_5 to Ambient Aerosol Particles, Environm. Sci. Technol., 48, 1618-1627, 10.1021/es4042622, 2014.

Ryder, O. S., Campbell, N. R., Morris, H., Forestieri, S., Ruppel, M. J., Cappa, C., Tivanski, A., Prather, K., and Bertram, T. H.: Role of Organic Coatings in Regulating N_2O_5 Reactive Uptake to Sea Spray Aerosol, J. Phys. Chem. A, 119, 11683-11692, 10.1021/acs.jpca.5b08892, 2015a.

Ryder, O. S., Campbell, N. R., Shaloski, M., Al-Mashat, H., Nathanson, G. M., and Bertram, T. H.: Role of Organics in Regulating $ClNO_2$ Production at the Air–Sea Interface, J. Phys. Chem. A, 119, 8519-8526, 10.1021/jp5129673, 2015b.

Sander, R., and Crutzen, P. J.: Model study indicating halogen activation and ozone destruction in polluted air masses transported to the sea, J. Geophys. Res., 101, 9121-9138, 10.1029/95JD03793, 1996.

Sander, S. P., Abbatt, J. P. D., Barker, J. R., Burkholder, J. B., Friedl, R. R., Golden, D. M., Huie, R. E., Kolb, C. E., Kurylo, M. J., Moortgat, G. K., Orkin, V. L., and Wine, P. H.: Chemical Kinetics and Photochemical Data for Use in Atmospheric Studies, Evaluation No. 17, JPL Publication 10-6, Jet Propulsion Laboratory, Pasadena, CA, 2010.

Sarwar, G., Simon, H., Xing, J., and Mathur, R.: Importance of tropospheric $ClNO_2$ chemistry across the Northern Hemisphere, Geophys. Res. Lett., 41, 4050-4058, 10.1002/2014gl059962, 2014.

Seinfeld, J. H., and Pandis, S. N.: Atmospheric chemistry and physics: from air pollution to climate change, 2nd ed., Wiley, Hoboken, N.J., 2006.

Simpson, W. R.: Continuous wave cavity ring-down spectroscopy applied to in situ detection of dinitrogen pentoxide (N_2O_5), Rev. Sci. Instrum., 74, 3442-3452, 10.1063/1.1578705, 2003.

1304 Slusher, D. L., Huey, L. G., Tanner, D. J., Flocke, F. M., and Roberts, J. M.: A thermal
1305 dissociation-chemical ionization mass spectrometry (TD-CIMS) technique for the
1306 simultaneous measurement of peroxyacyl nitrates and dinitrogen pentoxide, J. Geophys. Res.,
1307 109, D19315, 10.1029/2004JD004670, 2004.

1308 Steyn, D. G., Bottenheim, J. W., and Thomson, R. B.: Overview of tropospheric ozone in the
1309 Lower Fraser Valley, and the Pacific '93 field study, Atmos. Environm., 31, 2025-2035,
1310 10.1016/S1352-2310(97)00018-6, 1997.

1311 Stutz, J., Alicke, B., Ackermann, R., Geyer, A., Wang, S. H., White, A. B., Williams, E. J.,
1312 Spicer, C. W., and Fast, J. D.: Relative humidity dependence of HONO chemistry in urban
1313 areas, J. Geophys. Res., 109, D03307, 10.1029/2003JD004135, 2004a.

1314 Stutz, J., Alicke, B., Ackermann, R., Geyer, A., White, A., and Williams, E.: Vertical profiles
1315 of NO_3, N_2O_5, O_3, and NO_x in the nocturnal boundary layer: 1. Observations during the Texas
1316 Air Quality Study 2000, J. Geophys. Res., 109, D12306, doi:12310.11029/12003JD004209,
1317 2004b.

1318 Talbot, R., Mao, H. T., and Sive, B.: Diurnal characteristics of surface level O_3 and other
1319 important trace gases in New England, J. Geophys. Res., 110, D09307,
1320 doi:09310.01029/02004JD005449, 2005.

1321 Tanaka, P. L., Riemer, D. D., Chang, S. H., Yarwood, G., McDonald-Buller, E. C., Apel, E.
1322 C., Orlando, J. J., Silva, P. J., Jimenez, J. L., Canagaratna, M. R., Neece, J. D., Mullins, C. B.,
1323 and Allen, D. T.: Direct evidence for chlorine-enhanced urban ozone formation in Houston,
1324 Texas, Atmos. Environm., 37, 1393-1400, 10.1016/S1352-2310(02)01007-5 2003.

1325 Thaler, R. D., Mielke, L. H., and Osthoff, H. D.: Quantification of Nitryl Chloride at Part Per
1326 Trillion Mixing Ratios by Thermal Dissociation Cavity Ring-Down Spectroscopy, Anal.
1327 Chem., 83, 2761-2766, 10.1021/ac200055z, 2011.

Tham, Y., Yan, C., Xue, L., Zha, Q., Wang, X., and Wang, T.: Presence of high nitryl chloride in Asian coastal environment and its impact on atmospheric photochemistry, Chin. Sci. Bull., 59, 356-359, 10.1007/s11434-013-0063-y, 2014.

Tham, Y. J., Wang, Z., Li, Q., Yun, H., Wang, W., Wang, X., Xue, L., Lu, K., Ma, N., Bohn, B., Li, X., Kecorius, S., Größ, J., Shao, M., Wiedensohler, A., Zhang, Y., and Wang, T.: Significant concentrations of nitryl chloride sustained in the morning: investigations of the causes and impacts on ozone production in a polluted region of northern China, Atmos. Chem. Phys., 16, 14959-14977, 10.5194/acp-16-14959-2016, 2016.

Thieser, J., Schuster, G., Schuladen, J., Phillips, G. J., Reiffs, A., Parchatka, U., Pöhler, D., Lelieveld, J., and Crowley, J. N.: A two-channel thermal dissociation cavity ring-down spectrometer for the detection of ambient NO2, RO2NO2 and RONO2, Atmos. Meas. Tech., 9, 553-576, 10.5194/amt-9-553-2016, 2016.

Thornton, J. A., Kercher, J. P., Riedel, T. P., Wagner, N. L., Cozic, J., Holloway, J. S., Dube, W. P., Wolfe, G. M., Quinn, P. K., Middlebrook, A. M., Alexander, B., and Brown, S. S.: A large atomic chlorine source inferred from mid-continental reactive nitrogen chemistry, Nature, 464, 271-274, 10.1038/nature08905, 2010.

Tokarek, T. W., Huo, J. A., Odame-Ankrah, C. A., Hammoud, D., Taha, Y. M., and Osthoff, H. D.: A gas chromatograph for quantification of peroxycarboxylic nitric anhydrides calibrated by thermal dissociation cavity ring-down spectroscopy, Atmos. Meas. Tech., 7, 3263-3283, 10.5194/amt-7-3263-2014, 2014.

Trainer, M., Williams, E. J., Parrish, D. D., Buhr, M. P., Allwine, E. J., Westberg, H. H., Fehsenfeld, F. C., and Liu, S. C.: Models and observations of the impact of natural hydrocarbons on rural ozone, Nature, 329, 705-707, 10.1038/329705a0, 1987.

Tsai, C., Wong, C., Hurlock, S., Pikelnaya, O., Mielke, L. H., Osthoff, H. D., Flynn, J. H., Haman, C., Lefer, B., Gilman, J., de Gouw, J., and Stutz, J.: Nocturnal loss of NO_x during the 2010 CalNex-LA study in the Los Angeles Basin, J. Geophys. Res., 119, 13004–13025 10.1002/2014jd022171, 2014.

Vingarzan, R., and Li, S. M.: The Pacific 2001 Air Quality Study - synthesis of findings and policy implications, Atmos. Environm., 40, 2637-2649, 10.1016/j.atmosenv.2005.09.083, 2006.

Volpe, C., Wahlen, M., Pszenny, A. A. P., and Spivack, A. J.: Chlorine isotopic composition of marine aerosols: Implications for the release of reactive chlorine and HCl cycling rates, Geophys. Res. Lett., 25, 3831-3834, 10.1029/1998gl900038, 1998.

Wagner, N. L., Dube, W. P., Washenfelder, R. A., Young, C. J., Pollack, I. B., Ryerson, T. B., and Brown, S. S.: Diode laser-based cavity ring-down instrument for NO_3, N_2O_5, NO, NO_2 and O_3 from aircraft, Atmospheric Measurement Techniques, 4, 1227-1240, 10.5194/amt-4-1227-2011, 2011.

Wang, S., Ackermann, R., and Stutz, J.: Vertical profiles of O_3 and NO_x chemistry in the polluted nocturnal boundary layer in Phoenix, AZ: I. Field observations by long-path DOAS, Atmos. Chem. Phys., 6, 2671-2693, 10.5194/acp-6-2671-2006, 2006.

Wang, T., Tham, Y. J., Xue, L., Li, Q., Zha, Q., Wang, Z., Poon, S. C. N., Dubé, W. P., Blake, D. R., Louie, P. K. K., Luk, C. W. Y., Tsui, W., and Brown, S. S.: Observations of nitryl chloride and modeling its source and effect on ozone in the planetary boundary layer of southern China, J. Geophys. Res.-Atmos., 121, 2476-2489, 10.1002/2015jd024556, 2016.

Wang, X., Wang, H., Xue, L., Wang, T., Wang, L., Gu, R., Wang, W., Tham, Y. J., Wang, Z., Yang, L., Chen, J., and Wang, W.: Observations of N_2O_5 and $ClNO_2$ at a polluted urban

surface site in North China: High N_2O_5 uptake coefficients and low $ClNO_2$ product yields, Atmos. Environm., 156, 125-134, 10.1016/j.atmosenv.2017.02.035, 2017.

Wayne, R. P., Barnes, I., Biggs, P., Burrows, J. P., Canosamas, C. E., Hjorth, J., Lebras, G., Moortgat, G. K., Perner, D., Poulet, G., Restelli, G., and Sidebottom, H.: The Nitrate Radical - Physics, Chemistry, and the Atmosphere, Atmos. Environm. A, 25, 1-203, 10.1016/0960-1686(91)90192-A, 1991.

Wieser, M. E., and Berglund, M.: Atomic weights of the elements 2007 (IUPAC Technical Report), Pure Appl. Chem., 81, 2131-2156, 10.1351/pac-rep-09-08-03, 2009.

Wild, R. J., Dubé, W. P., Aikin, K. C., Eilerman, S. J., Neuman, J. A., Peischl, J., Ryerson, T. B., and Brown, S. S.: On-road measurements of vehicle NO_2/NO_x emission ratios in Denver, Colorado, USA, Atmos. Environm., 148, 182-189, 10.1016/j.atmosenv.2016.10.039, 2017.

Wood, E. C., Bertram, T. H., Wooldridge, P. J., and Cohen, R. C.: Measurements of N_2O_5, NO_2, and O_3 east of the San Francisco Bay, Atmos. Chem. Phys., 5, 483-491, 10.5194/acp-5-483-2005, 2005.

Young, C. J., Washenfelder, R. A., Roberts, J. M., Mielke, L. H., Osthoff, H. D., Tsai, C., Pikelnaya, O., Stutz, J., Veres, P. R., Cochran, A. K., VandenBoer, T. C., Flynn, J., Grossberg, N., Haman, C. L., Lefer, B., Stark, H., Graus, M., de Gouw, J., Gilman, J. B., Kuster, W. C., and Brown, S. S.: Vertically Resolved Measurements of Nighttime Radical Reservoirs in Los Angeles and Their Contribution to the Urban Radical Budget, Environm. Sci. Technol., 46, 10965-10973, 10.1021/es302206a, 2012.

Young, C. J., Washenfelder, R. A., Edwards, P. M., Parrish, D. D., Gilman, J. B., Kuster, W. C., Mielke, L. H., Osthoff, H. D., Tsai, C., Pikelnaya, O., Stutz, J., Veres, P. R., Roberts, J. M., Griffith, S., Dusanter, S., Stevens, P. S., Flynn, J., Grossberg, N., Lefer, B., Holloway, J. S., Peischl, J., Ryerson, T. B., Atlas, E. L., Blake, D. R., and Brown, S. S.: Chlorine as a

primary radical: evaluation of methods to understand its role in initiation of oxidative cycles, Atmos. Chem. Phys., 14, 3427-3440, 10.5194/acp-14-3427-2014, 2014.

Zhang, Q., Jimenez, J. L., Worsnop, D. R., and Canagaratna, M.: A case study of urban particle acidity and its influence on secondary organic aerosol, Environm. Sci. Technol., 41, 3213-3219, 10.1021/es061812j, 2007.

1405 **Table 1**. Summary of measurement techniques deployed at T45 during the study.

Species or parameter	Method	Uncer-tainty	Time resolution
$ClNO_2$, PAN, PPN	Chemical ionization mass spectrometry (Mielke et al., 2011)	±25% ±10%	30 s
N_2O_5	Red diode laser cavity ring-down spectroscopy (Odame-Ankrah and Osthoff, 2011)	±25%	1 s
O_3	UV absorption (Thermo 49i)	±10%	10 s
NO/NO_y	O_3-Chemiluminescence (Thermo 42i-Y) with heated Mo converter; operated with inlet filter	±30%	10 s
NO_2	Blue diode laser cavity ring-down spectroscopy (Paul and Osthoff, 2010)	±10%	1 s
PAN, PPN	Gas chromatography with electron capture detection (Tokarek et al., 2014)	±10%	6 min
Photolysis frequencies	Spectral radiometry (Metcon)	±20%	10 s
Aerosol size distribution	Scanning mobility particle sizer (SMPS)		nd
Aerosol composition	Aerosol Chemical Speciation Monitor (ACSM)	±20%	30 min
VOCs	Agilent	±30%	20 min (1 hr*)
Meteorological data	Various		

1406 * Sampled for 20 min within a 1 hour time period

Table 2. Ratios of up- to down-welling photolysis frequencies.

Frequency	Ratio
$j(NO_3)$	0.27±0.04
$j(NO_2)$	0.15±0.03
$j(ClNO_2)$	0.14±0.02
$j(O_3 \rightarrow O(^1D))$	0.11±0.02

1409 **Table 3**. Maximum $ClNO_2$ mixing ratios observed to date.

Location	Type	Maximum mixing ratio	Reference(s)
Houston, TX	Off-shore, costal, and inland	1.2 ppbv	(Osthoff et al., 2008)
New England	Off-shore	90 pptv	(Kercher et al., 2009)
Pasadena, CA	Off-shore	2.15 ppbv	(Riedel et al., 2012a)
La Jolla, CA	Coastal	30 pptv	(Kim et al., 2014)
Boulder, CO	Continental	425 pptv	(Thornton et al., 2010)
Calgary, AB	Continental	330 pptv	(Mielke et al., 2016; Mielke et al., 2011)
Erie, CO	Continental	1.3 ppbv	(Riedel et al., 2013; Brown et al., 2013)
Feldberg, GER	Continental	800 pptv	(Phillips et al., 2012; Phillips et al., 2016)
Horsepool, UT	Continental	500 pptv	(Edwards et al., 2014)
Pasadena, CA	Coastal, inland	3.5 ppbv	(Mielke et al., 2013)
London, UK	Coastal, inland	724 pptv	(Bannan et al., 2015)
Hongkong, PRC	Coastal, inland	2.0 ppbv	(Tham et al., 2014)
Southeast TX	Coastal, inland	280 pptv	(Faxon et al., 2015)
Hongkong, PRC	Coastal, inland	4.7 ppbv	(Wang et al., 2016)
North China Plain	Continental	2.1 ppbv	(Tham et al., 2016)
North China Plain	Continental	776 pptv	(Wang et al., 2017)
Abbotsford, BC	Coastal, inland	97 pptv	This work

1410